Received: 12 October 2021 | Revised: 22 March 2022 | Accepted: 30 April 2022

DOI: 10.1002/jev2.12232

RESEARCH ARTICLE

A multi-omics approach identifies pancreatic cancer cell extracellular vesicles as mediators of the unfolded protein response in normal pancreatic epithelial cells

Charles P. Hinzman[1] | Baldev Singh[2] | Shivani Bansal[2] | Yaoxiang Li[2] | Anton Iliuk[3] | Michael Girgis[2] | Kelly M. Herremans[4] | Jose G. Trevino[5] | Vijay K. Singh[6,7] | Partha P. Banerjee[1] | Amrita K. Cheema[1,2]

[1]Department of Biochemistry, Molecular and Cellular Biology, Georgetown University Medical Centre, Washington, DC, USA

[2]Department of Oncology, Lombardi Comprehensive Cancer Center, Georgetown University Medical Centre, Washington, DC, USA

[3]Tymora Analytical Operations, West Lafayette, IN, USA

[4]Department of Surgery, University of Florida, Gainesville, FL, USA

[5]Division of Surgical Oncology, VCU Massey Cancer Centre, Richmond, VA, USA

[6]Department of Pharmacology and Molecular Therapeutics, School of Medicine, Uniformed Services University of the Health Sciences, Bethesda, MD, USA

[7]Armed Forces Radiobiology Research Institute, Uniformed Services University of the Health Sciences, Bethesda, MD, USA

Correspondence
Amrita Cheema, GC2, Pre-Clinical Science Building, 3900 Reservoir Road NW, Washington, DC 20057, USA.
Email: akc27@georgetown.edu

Funding information
NCI, Grant/Award Number: P30-CA051008; NIH, Grant/Award Number: G20-RR31199; American Cancer Society, Grant/Award Numbers: IRG-92-152-17, AWD4470404; National Center for Advancing Translational Sciences, Grant/Award Number: TL1TR001431; Cosmos Club Foundation; Ruesch Family Foundation

Abstract
Although cancer-derived extracellular vesicles (cEVs) are thought to play a pivotal role in promoting cancer progression events, their precise effect on neighbouring normal cells is unknown. In this study, we investigated the impact of pancreatic cancer ductal adenocarcinoma (PDAC) derived EVs on recipient non-tumourigenic pancreatic normal epithelial cells upon internalization. We demonstrate that cEVs are readily internalized and induce endoplasmic reticulum (ER) stress and the unfolded protein response (UPR) in treated normal pancreatic epithelial cells within 24 h. We further show that PDAC cEVs increase cell proliferation, migration, and invasion and that these changes are regulated at least in part, by the UPR mediator DDIT3. Subsequently, these cells release several inflammatory cytokines. Leveraging a layered multi-omics approach, we analysed EV cargo from a panel of six PDAC and two normal pancreas cell lines, using multiple EV isolation methods. We found that cEVs were enriched for an array of biomolecules which can induce or regulate ER stress and the UPR, including palmitic acid, sphingomyelins, metabolic regulators of tRNA charging and proteins which regulate trafficking and degradation. We further show that palmitic acid, at doses relevant to those found in cEVs, is sufficient to induce ER stress in normal pancreas cells. These results suggest that cEV cargo packaging may be designed to disseminate proliferative and invasive characteristics upon internalization by distant recipient normal cells, hitherto unreported. This study is among the first to highlight a major role for PDAC cEVs to induce stress in treated normal pancreas cells that may modulate a systemic response leading to altered phenotypes. These findings highlight the importance of EVs in mediating disease aetiology and open potential areas of investigation toward understanding the role of cEV lipids in promoting cell transformation in the surrounding microenvironment.

KEYWORDS
ER stress, extracellular vesicles, multi-omics, pancreatic cancer

This is an open access article under the terms of the Creative Commons Attribution-NonCommercial-NoDerivs License, which permits use and distribution in any medium, provided the original work is properly cited, the use is non-commercial and no modifications or adaptations are made.
© 2022 The Authors. *Journal of Extracellular Vesicles* published by Wiley Periodicals, LLC on behalf of the International Society for Extracellular Vesicles.

1 | INTRODUCTION

Pancreatic cancer is projected to become the 2nd leading cause of cancer-related mortality in the United States and Europe by 2030 (Quante et al., 2016; Rahib et al., 2014). The estimated 5-year survival rate currently remains ∼11% (Siegel et al., 2020). Two key drivers of these poor outcomes are increasing incidence (the number of patients diagnosed each year has doubled over the last 20 years) and late-stage diagnosis (Siegel et al., 2020). Pancreatic ductal adenocarcinoma (PDAC) is the most common type of pancreatic cancer. Unfortunately, 80% of patients with this lethal malignancy are ineligible for surgical resection due to late-stage disease at diagnosis (Hartwig et al., 2013; Renz et al., 2017). Though key genetic alterations are known to coincide with disease progression, this knowledge has not led to the development of early detection assays (Cicenas et al., 2017). A key feature in PDAC is the diversity of cell types in the tumour microenvironment; as much as 90% of the tumour volume can consist of non-cancer cells (Neesse et al., 2011). In recent years, several studies have sought to understand the role of various cell types in the tumour microenvironment and the interaction between PDAC tumour cells and other cell populations, including cancer associated fibroblasts (CAFs) (Elyada et al., 2019; Öhlund et al., 2017; Vennin et al., 2019), immune cells (Balachandran et al., 2019; Blando et al., 2019; Padoan et al., 2019) and endothelial cells (Masamune et al., 2008; Morin et al., 2018). Importantly, complex intercellular communication is needed to facilitate coordinated efforts that are conducive to tumour growth. While these studies demonstrate how different cell types may harmonize with cancer cells for disease progression, many of these are focused on very late stages of disease, often when patients have few treatment options. A better understanding of mediators of early formation of the tumour microenvironment is critical for improving clinical outcomes in pancreatic cancer.

Extracellular vesicles (EVs) are heterogeneous nanometre to micrometre sized lipid-bilayer particles released from cells of all tissue types (El Andaloussi et al., 2013; Shah et al., 2018; Willms et al., 2018). EVs play important signal mediating roles in a variety of normal physiological processes, as well as in several pathologies, including cancer (Bouvy et al., 2014; Maacha et al., 2019; Xu et al., 2018; Yáñez-Mó et al., 2015). EV cargo is a rich source of potential biomarkers for PDAC diagnosis (Allenson et al., 2017; Lennon et al., 2019; Yu et al., 2020) and can mediate survival signalling between CAFs and cancer cells (Richards et al., 2017; Zhao et al., 2016). EVs also suppress the immune system in the tumour microenvironment and can prime metastatic sites for pre-cancer cell infiltration (Chang et al., 2020; Costa-Silva et al., 2015; Yin et al., 2019). Although these studies suggest that EVs likely regulate intercellular communication within the late-stage tumour microenvironment, few studies have attempted to address the role of EVs in mediating the earliest stages of PDAC development. Herein, we tested the hypothesis that PDAC EVs could mediate distinct biochemical, genetic, or metabolic alterations in treated normal pancreatic epithelial cells. Using a systematic multi-pronged omics approach, we show that PDAC cell-derived EVs (cEVs) induce a myriad of stress response pathways in treated normal pancreatic epithelial cells. These events culminate in activation of the unfolded protein response, driving inflammation and altered cell behaviour. These studies highlight a novel stress activation paradigm by which cEVs may prime the microenvironment driving disease onset and ultimately tumour progression.

2 | RESULTS

2.1 | Key differences exist between extracellular vesicles isolated from pancreas cancer cell lines compared to normal pancreas cell lines

To validate our EV isolation methods, we characterized our sample preparations using orthogonal techniques including immunoblot analysis, cryogenic electron microscopy (Cryo-EM) and nanoparticle tracking analysis (NTA). One of the striking observations was the differential expression of certain "canonical" EV markers between pancreas cancer and normal cells. EVs isolated from the normal cell line hTERT-HPNE (an established immortalized non-tumourigenic pancreas cell line), for example, did not express the Programmed cell death 6-interacting protein (PDCD6IP), also known as ALG-2-interacting protein (ALIX) (Figure 1a). Cargo sorting into small EVs involves many proteins within the endosomal sorting complex required for transport (ESCRT) pathway, such as ALIX, and thus it is commonly used as a marker for exosomes (Willms et al., 2016). Furthermore, EVs isolated from the cancer cell line MiaPaCa-2 did not express epithelial cell adhesion molecule (EPCAM) (Figure 1a), another widely used marker for exosomes. Interestingly, normal cell EVs expressed certain markers higher than tumour cell EVs, such as cluster of differentiation 81 (CD81) which is highly expressed in hTERT-HPNE EVs (Figure 1a). Taken together, these differences underscore the importance of assessing various protein markers when isolating EVs from samples, as there appears to be heterogeneous expression of commonly used EV-specific proteins across cell lines.

Quantifying EVs using nanoparticle tracking analysis (NTA), we found that pancreatic cancer cells on average secreted 2-8-fold more EVs compared to normal pancreatic cells (Figure 1b). Furthermore, NTA showed that EVs isolated from all the eight cell lines used in our study differed in terms of average particle diameter, ranging from ∼144 nm in HPDE-H6c7 cells to ∼325 nm in Capan-1 cells. (Figure 1c), an initial observation we continue to investigate. Given the differences in the median diameter observed using NTA and cryo-EM across different cell lines, our methods of EV enrichment may be capturing EV subpopulations including exosomes and microvesicles (Willms et al., 2018). Finally, we observed that the enriched EV fraction

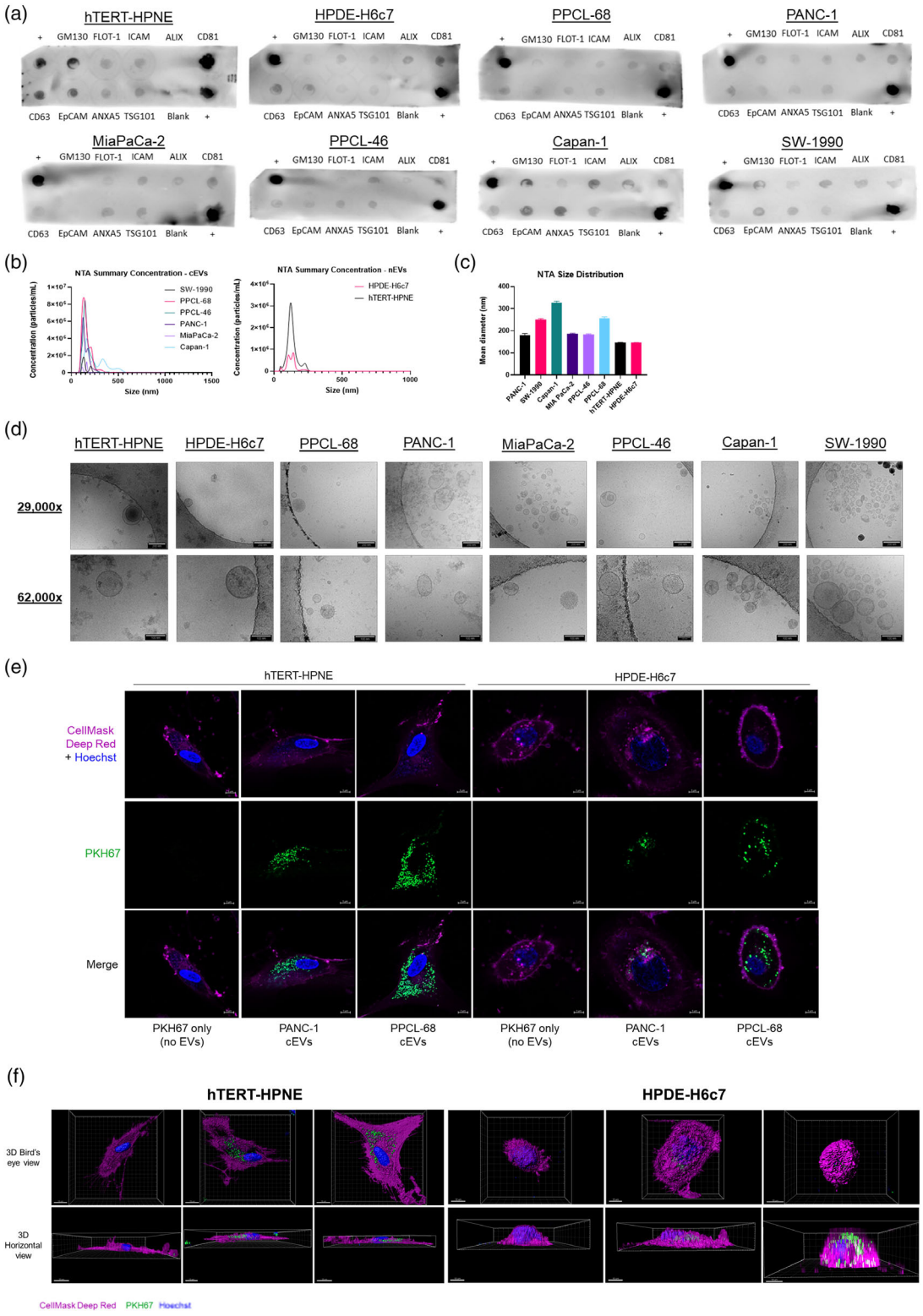

FIGURE 1 Extracellular vesicles derived from pancreas cancer cells significantly differ from normal pancreas cells EVs and are readily internalized by treated normal cells. (a) Immunoblot arrays comparing the expression of known EV markers in EVs isolated from the normal pancreas cell lines hTERT-HPNE, HPDE-H6c7 and the pancreas cancer cell lines PPCL-68, PANC-1, MiaPaCa-2, PPCL-46, Capan-1 and SW-1990. (b) Nanoparticle tracking analysis (NTA) concentration data of cancer-cell EVs (cEVs, left) and normal-cell EVs (nEVs, right) demonstrating key differences in EV yield. (c) Mean diameter size for each EV preparation, as determined by NTA. $N = 3$ independent EV isolations per cell line. (d) Representative cryogenic electron microscopy images from EV preparations at medium (29,000x) and high (62,000x) magnifications. Scale bar is 200 nm. (e) Representative confocal microscopy images and (f) 3D IMARIS reconstructions of acquired Z-stack confocal images of hTERT-HPNE or HPDE-H6c7 cells treated with PANC-1 or PPCL-68 cEVs dyed with PKH67 (green). Nuclei stained with Hoechst 33342 (blue) and cell membranes stained with CellMask Deep Red (magenta). Images acquired at 63x magnification. PKH67 added to 1 x PBS without any EVs was used as a negative control to ensure green fluorescent signal was not generated by dye aggregates.

had visible lipid bilayers and expected vesicle morphology using cryo-EM (Figure 1d). These results highlight the importance of characterizing EV samples isolated from various cell culture lines using multiple approaches, to identify key differences in EV populations.

2.2 | cEVs induce significant gene expression changes in treated normal pancreatic epithelial cells

To investigate how cEVs may regulate treated normal cells, we analysed global gene expression changes in cEV treated normal cells using RNA-Seq. Initially, we performed EV internalization experiments, to ensure that cEVs were internalized by cEV treated normal cells. After isolation, cEVs were labelled using the lipid-anchored fluorophore PKH67. As previous publications have demonstrated various issues with fluorescent labelling of EVs (Pužar Dominkuš et al., 2018; Simonsen, 2019; Takov et al., 2017), we generated dummy samples wherein PKH67 was added to PBS containing no EVs, to help rule out generation of fluorescent signal due to the formation of dye aggregates. Using low resolution fluorescence microscopy, we initially observed that both cEVs isolated from PANC-1 and PPCL-68 cells, a patient-derived xenograft (PDX) cell line (Pham et al., 2016) seemed to be internalized by HPDE-H6c7 and hTERT-HPNE cells (Figure S1). We confirmed internalization using high resolution confocal microscopy. Treatment of normal cells with either PANC-1 or PPCL-68 cEVs stained with PKH67 (green) showed significant enrichment in the intracellular space (Figure 1e). We did not observe dye aggregate formation using PKH67 without EVs as a control. 3D rendering and analysis of the Z-stack acquisition with IMARIS unambiguously demonstrated that cEVs were contained within the cells; interestingly we observed concentration of EVs around the perinuclear space (Figure 1f, Videos S1–S6).

We next treated hTERT-HPNE and HPDE-H6c7 ($n = 3$ per group), with cEVs from PANC-1 and PPCL-68 PDAC cells or a negative control (residual media left behind after enrichment of cEVs by ultracentrifugation) for 24 h and performed RNA-Seq to measure gene expression changes. Visualization of gene expression using MA plots indicated robust change in the global gene expression profiles of both HPDE-H6c7 and hTERT-HPNE cells 24 h post cEV treatment (Figure 2a).

Gene set enrichment analysis (GSEA) identified 1005 and 3259 differentially expressed genes (DEGs) (FDR-adj. $p < 0.05$, see methods) in hTERT-HPNE and HPDE-H6c7 cells, respectively (Figure 2b, Data S1). We found 376 DEGs commonly dysregulated in both cell lines in response to both cEV treatments, but not in the negative control group. Next, we performed protein-protein interaction network analysis using the Search Tool for the Retrieval of Interacting Genes/Proteins (STRING) database (Snel, 2000; Szklarczyk et al., 2021). Of the 376 DEGs, 252 were upregulated; this gene set had significant protein-protein interactions (PPI enrichment $p = 2.09\text{e-}07$) (Figure 2c), containing genes in the aminoacyl-tRNA biosynthesis (adj. $p = 2.69\text{e-}05$), cytosolic tRNA aminoacylation (adj. $p = 1.19\text{e-}06$) and ATF4 (adj. $p = 0.0402$)/ATF6 (adj. $p = 0.0402$) pathways. We separately analysed the remaining 124 genes which were downregulated. Interestingly, these genes similarly exhibited significantly increased protein-protein interaction (PPI enrichment $p = 0.00528$) particularly for genes involved in protein refolding (adj. $p = 0.0087$) (Figure S2). Overall, Gene ontology (GO) analysis of the 376 common DEGs suggested enrichment in biological processes associated with endoplasmic reticulum (ER) stress, nuclear factor kappa-light-chain-enhancer of activated B cells (NF-κB) signalling, cytokine production and response to DNA damage (Figure 2d, Data S2). Lipid synthesis seemed to be significantly dysregulated, with decreased expression in genes regulating cholesterol, sterol, and acetyl-CoA synthesis pathways (Figure 2d, Data S2). Taken together, these findings indicate that normal pancreatic cells undergo distinct stress responses after cEV treatment, altering the biosynthesis of lipid species.

Though widely used as normal pancreatic cell models, hTERT-HPNE and HPDE-H6c7 lines differ in origin, method of immortalization, and morphology. We analysed DEGs uniquely dysregulated in each cell line to examine cell line specific responses to cEV treatment. In HPDE-H6c7 cells, a model better representing a true epithelial cell, pathway analysis revealed enrichment in the unfolded protein response (UPR) and ER stress signalling, inositol metabolism and adipocytokine signalling (Figure S2, Data S3), whereas cell cycle pathways were down-regulated (Figure S2, Data S3). Interestingly, in hTERT-HPNE cells, an intermediate acinar-to-ductal metaplasia state cell model, we again found that cEVs increased expression of genes regulating UPR/ER stress (including TNF Receptor Associated Factor 6 (*TRAF6*)-mediated Interferon Regulatory Factor 7 (*IRF7*) activation), but also hippo, tumour necrosis factor-alpha (TNF-α) and interferon-gamma (IFN-γ) signalling (Figure S2, Data S3). Lipid biosynthesis, transforming growth factor-beta (TGF-β)-dependent extracellular matrix regulation and NOTCH signalling were down-regulated (Figure S2, Data S3). These results highlight that individual cell lines differentially respond to cEV treatment, though the induction of UPR/ER stress seemed to be a consistent theme between these models underscoring the biological relevance and significance of this pathway perturbation in the treated cells.

2.3 | cEVs induce the unfolded protein response and ER stress in treated normal pancreatic epithelial cells

Given that the UPR/ER stress pathway was predominant in the GO analysis of both common and unique DEGs, and implicated in our STRING analysis, this warranted further investigation. Motif analysis using the Hypergeometric Optimization of

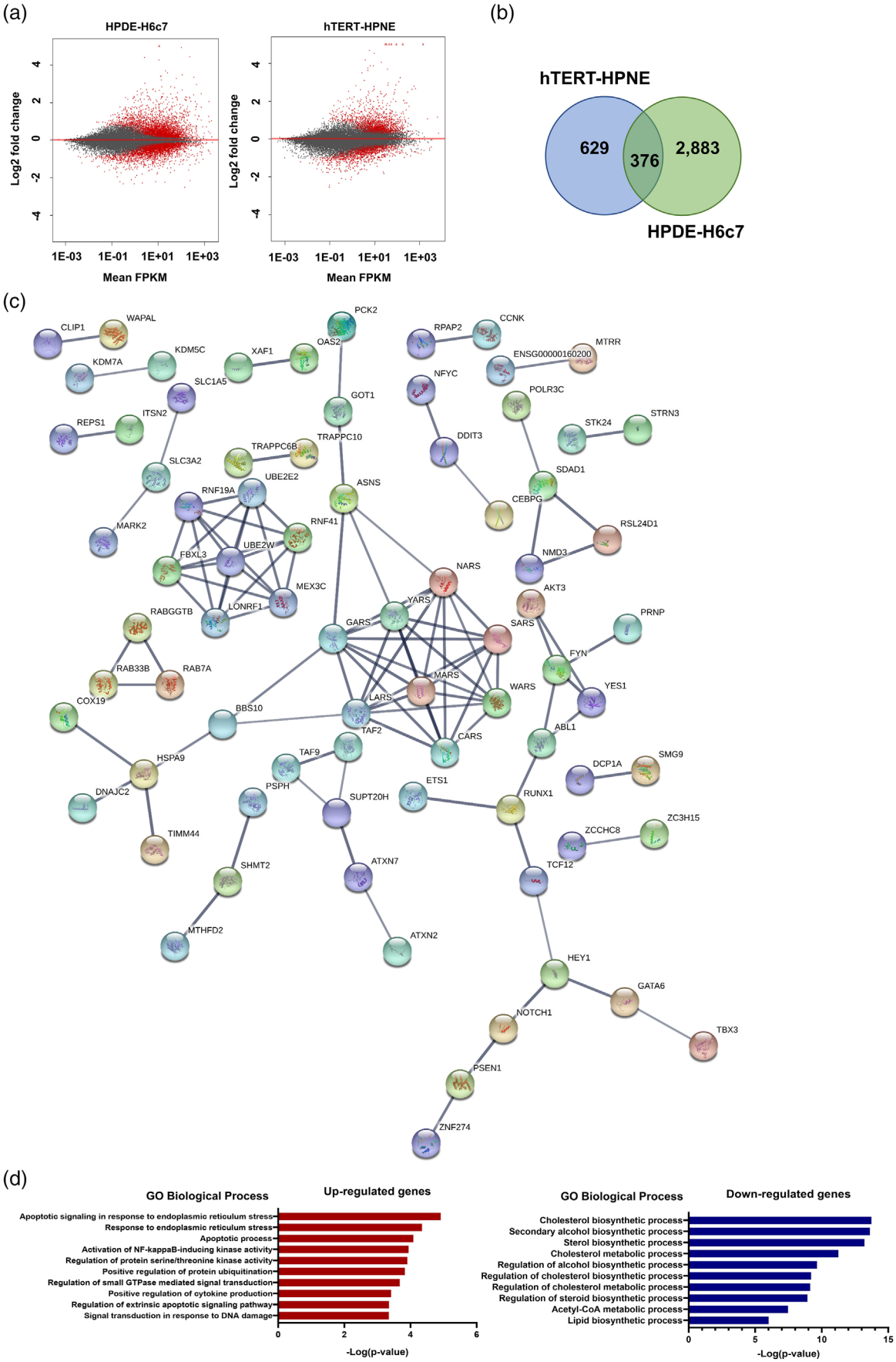
(a)
HPDE-H6c7
hTERT-HPNE
Log2 fold change
Mean FPKM
1E-03
1E-01
1E+01
1E+03
(b)
hTERT-HPNE
629
376
2,883
HPDE-H6c7
(c)
CLIP1
WAPAL
KDM5C
KDM7A
SLC1A5
ITSN2
REPS1
SLC3A2
MARK2
PCK2
OAS2
XAF1
GOT1
TRAPPC10
TRAPPC6B
UBE2E2
RNF19A
RNF41
UBE2W
FBXL3
MEX3C
LONRF1
RABGGTB
RAB33B
RAB7A
COX19
BBS10
HSPA9
DNAJC2
TIMM44
ASNS
RPAP2
CCNK
MTRR
ENSG00000160200
NFYC
POLR3C
DDIT3
STK24
STRN3
SDAD1
CEBPG
RSL24D1
NMD3
AKT3
PRNP
NARS
YARS
GARS
SARS
MARS
LARS
WARS
CARS
TAF2
TAF9
PSPH
SUPT20H
FYN
YES1
ABL1
DCP1A
SMG9
ETS1
RUNX1
ZCCHC8
ZC3H15
TCF12
SHMT2
MTHFD2
ATXN7
ATXN2
HEY1
GATA6
NOTCH1
TBX3
PSEN1
ZNF274
(d)
GO Biological Process
Up-regulated genes
Apoptotic signaling in response to endoplasmic reticulum stress
Response to endoplasmic reticulum stress
Apoptotic process
Activation of NF-kappaB-inducing kinase activity
Regulation of protein serine/threonine kinase activity
Positive regulation of protein ubiquitination
Regulation of small GTPase mediated signal transduction
Positive regulation of cytokine production
Regulation of extrinsic apoptotic signaling pathway
Signal transduction in response to DNA damage
0
2
4
6
-Log(p-value)
GO Biological Process
Down-regulated genes
Cholesterol biosynthetic process
Secondary alcohol biosynthetic process
Sterol biosynthetic process
Cholesterol metabolic process
Regulation of alcohol biosynthetic process
Regulation of cholesterol biosynthetic process
Regulation of cholesterol metabolic process
Regulation of steroid biosynthetic process
Acetyl-CoA metabolic process
Lipid biosynthetic process
0
5
10
15
-Log(p-value)

Motif EnRichment (HOMER) platform (Heinz et al., 2010) showed the DEG gene set preferentially contained target motifs of C/EBP homologous protein (*CHOP)*, also known as DNA damage-inducible transcript 3 (*DDIT3*) (Figure 3a). Additional transcription factor analysis using the Enrichr platform (Chen et al., 2013; Kuleshov et al., 2016) confirmed this observation (Figure 3b). DDIT3/CHOP is a key transcription factor upregulated in response to elevated UPR (Cao et al., 2019; Lu et al., 2014). Transcriptional regulatory network analysis further identified overrepresentation of key regulatory elements targeted by several transcription factors responsible for regulating UPR/ER stress, including *DDIT3*, X-Box Binding Protein 1 (*XBP1)*, Hypoxia Inducible Factor 1 Subunit Alpha *(HIF1A)*, and Activating Transcription Factors 6, 4 and 3 *(ATF6, ATF4 and ATF3)* (Figure 3b, Figure S3). In the UPR/ER stress pathways, the leading genes enriched in our dataset (*DDIT3*, Heat Shock Protein Family A (Hsp70) Member 5 *(HSPA5)*, Nuclear Transcription Factor Y Subunit Beta *(NFYB)*, Nuclear Transcription Factor Y Subunit Gamma *(NFYC), ATF6* and *ATF4)* were upregulated post cEV treatment (Figure 3c) suggesting cEVs induce the UPR in treated normal cells.

Next, we validated these findings using qPCR. In independent experiments, we treated both normal cell lines (hTERT-HPNE and HPDE-H6c7) with separate batches of cEVs derived from PANC-1 or PPCL-68 PDAC cells, as well as the residual media used as a negative control. We confirmed up-regulation of key UPR and ER stress regulators including *XBP1, DDIT3*, Endoplasmic Reticulum to Nucleus Signalling 1 *(ERN1)*, Protein phosphatase 1 regulatory subunit 15A (*PPP1R15A)*, also known as Growth Arrest and DNA-Damage-Inducible 34 (*GADD34)*, Homocysteine Inducible ER Protein with Ubiquitin Like Domain 1 *(HERPUD1)* and Stress Associated Endoplasmic Reticulum Protein 1 *(SERP1)* (Figure 3d). We further validated ER stress induction using hTERT-HPNE and HPDE-H6c7 cell lines stably transfected with an ER Stress Response Element (ERSE) luciferase reporter. After cEV treatment, there was significant upregulation in ERSE-reporter activity in both cell lines (Figure 3e).

To further evaluate induction of the UPR at the protein level, we examined protein expression of key UPR mediators including CHOP/DDIT3, the spliced (XBP1s) and unspliced (XBP1u) variants of XBP1, Eukaryotic Translation Initiation Factor 2 Alpha Kinase 3 (EIF2AK3)/PERK, ATF6, Endoplasmic Reticulum to Nucleus Signalling 1 (ERN1)/Inositol-Requiring Enzyme 1 (IRE1) and phosphorylated ERN1/IRE1 (S724) after cEV treatment. Using cEVs and normal cell EVs (nEVs) isolated using a separate size-exclusion chromatography (SEC)-based method, we found that CHOP/DDIT3, XBP1s, and XBP1u were all significantly upregulated 24 h post-cEV treatment in both HPDE-H6c7 and hTERT-HPNE cells (Figure 3f). EIF2AK3/PERK and ATF6 were both upregulated in HPDE-H6c7 cells, but not as strongly in hTERT-HPNE cells (Figure 3f). ERN1/IRE1 and phosphorylated ERN1/IRE1 (S724) were both significantly upregulated in HPDE-H6c7 cells post-cEV treatment (Figure 3g). These findings confirmed that ER stress and the UPR was directly induced by uptake of cEVs regardless of EV isolation method.

Though we observed some increase in the protein expression of certain targets with nEVs, their induction did not seem to activate the UPR. When treating cells with cEVs isolated using the SEC method, ERSE luciferase activity was significantly increased, whereas treatment with nEVs isolated from normal hTERT-HPNE cells did not induce ERSE luciferase activity (Figure 3h). Furthermore, we observed ER stress induction using a lower dose of cEVs, persisting 48 h post treatment (Figure 3h, Figure S4). Taken together, these data suggest that UPR/ER stress induction is independent of cEV isolation method, is dose dependent and is specific to pancreatic cancer cell EVs.

Since prolonged ER stress and the UPR can induce inflammation, we performed a time course experiment to see if cEV treated normal cells released inflammatory cytokines. We found that 2 and 4 days post-cEV treatment, treated normal cells secreted significantly higher levels of fibroblast growth factor 2 (FGF2) and granulocyte-macrophage colony-stimulating factor (GM-CSF) (Figure 3i). However, treatment with nEVs isolated from the normal cell line, hTERT-HPNE, did not result in increased cytokine release, again suggesting this response is specific to cEVs. Prolonged ER stress can also induce apoptosis, specifically in the context of higher CHOP/DDIT3 expression (Hu et al., 2018). Therefore, we next investigated whether treated normal cells underwent increased apoptosis. We performed Annexin V and propidium iodide (PI) staining of cEV treated normal cells and sorted them by flow cytometry to quantify the fraction of cells undergoing apoptosis. There was no significant difference between the percentage of apoptotic or late apoptotic cells either 24 or 48 h post-cEV treatment (Figure 3j), suggesting no increased apoptosis in cEV treated cells. We further examined cell death by measuring caspase 3/7 activity, live/dead cell staining and

FIGURE 2 Pancreas cancer cell extracellular vesicles (cEVs) induce robust gene expression changes in treated normal pancreas cells. (a) MA plots showing robust gene expression changes in HPDE-H6c7 (left) and hTERT-HPNE (right) cells post-24-h treatment with PANC-1 cEVs. Red dots indicate genes which are significantly dysregulated (FDR-adj. $p < 0.05$ and fold-change <0.5 or >2, $n = 3$ per condition). (b) Number of significantly differentially expressed genes in hTERT-HPNE and HPDE-H6c7 cells after 24-h treatment with cEVs. (c) STRING analysis visualizing protein-protein interactions between upregulated common DEGs in hTERT-HPNE and HPDE-H6c7 cells (PPI-enrichment p-value = 2.09e-07). Line thickness represents confidence of the interaction and only high-confidence interactions are shown. Unconnected nodes are hidden. This network was enriched for genes in the aminoacyl-tRNA biosynthesis (adj. $p = 2.69e-05$), cytosolic tRNA aminoacylation (adj. $p = 1.19e-06$) and ATF4 (adj. $p = 0.0402$)/ATF6 (adj. $p = 0.0402$) pathways. (d) Gene ontology (GO) biological process classification of the 376 common DEGs between hTERT-HPNE and HPDE-H6c7 cells. These genes were enriched in biological processes regulating endoplasmic reticulum (ER) stress, NF-kB signalling, cytokine production and response to DNA damage, while lipid synthesis was severely altered, with decreased expression in genes regulating several cholesterol, sterol and acetyl-CoA synthesis pathways. FDR-adjusted $p < 0.05$ was used to select significant pathways and -log (p-value) was used for visualization.

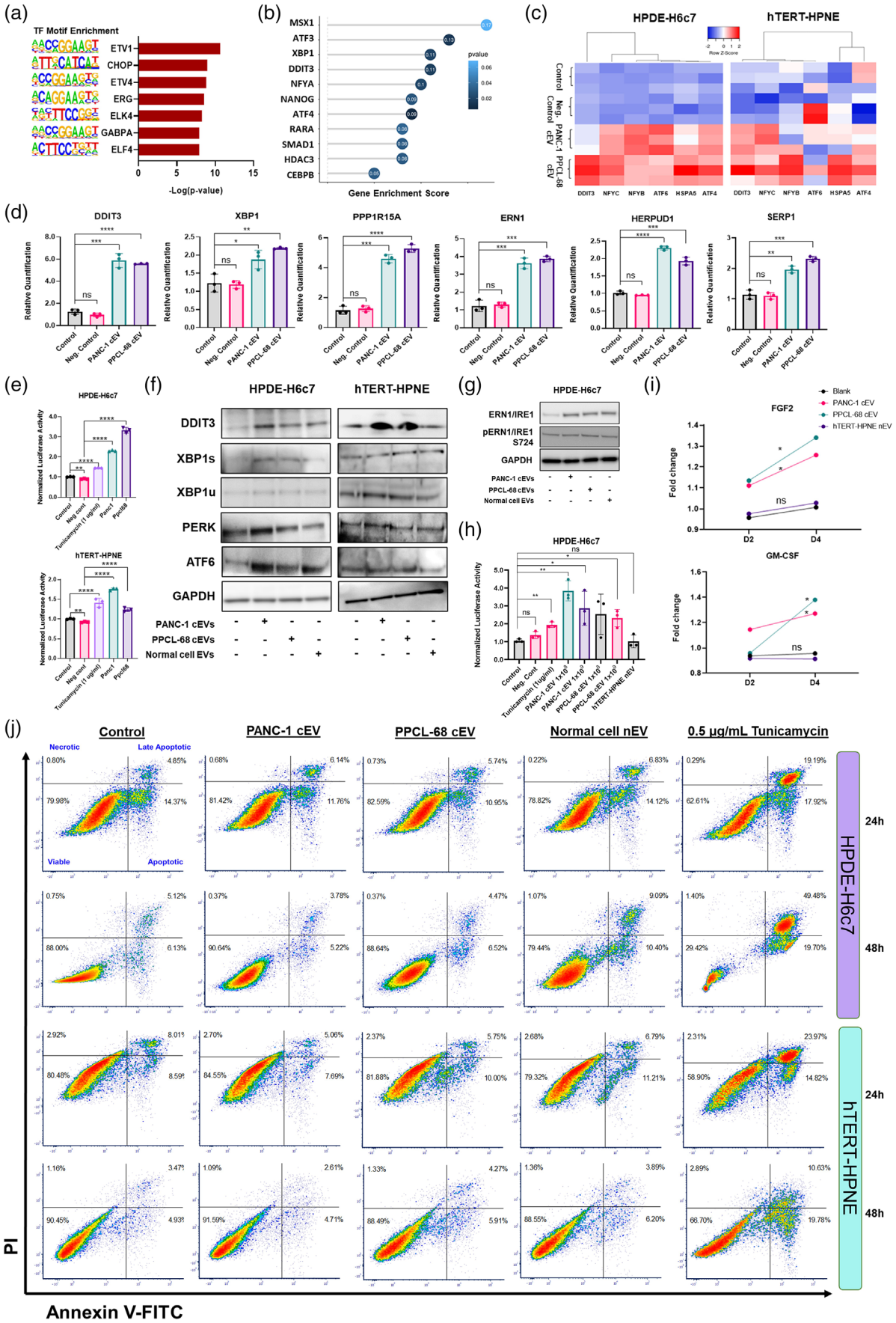
(a)
TF Motif Enrichment
ETV1
CHOP
ETV4
ERG
ELK4
GABPA
ELF4
-Log(p-value)
(b)
MSX1
ATF3
XBP1
DDIT3
NFYA
NANOG
ATF4
RARA
SMAD1
HDAC3
CEBPB
pvalue
Gene Enrichment Score
(c)
HPDE-H6c7
hTERT-HPNE
Control
Neg. Control
PANC-1 cEV
PPCL-68 cEV
DDIT3
NFYC
NFYB
ATF6
HSPA5
ATF4
(d)
DDIT3
XBP1
PPP1R15A
ERN1
HERPUD1
SERP1
Relative Quantification
Control
Neg. Control
PANC-1 cEV
PPCL-68 cEV
(e)
HPDE-H6c7
hTERT-HPNE
Normalized Luciferase Activity
Control
Neg cont
Tunicamycin (1 ug/ml)
Panc1
Ppcl68
(f)
HPDE-H6c7
hTERT-HPNE
DDIT3
XBP1s
XBP1u
PERK
ATF6
GAPDH
PANC-1 cEVs
PPCL-68 cEVs
Normal cell EVs
(g)
HPDE-H6c7
ERN1/IRE1
pERN1/IRE1 S724
GAPDH
PANC-1 cEVs
PPCL-68 cEVs
Normal cell EVs
(h)
HPDE-H6c7
Normalized Luciferase Activity
Control
Neg. Cont
Tunicamycin (1ug/ml)
PANC-1 cEV 1x10^9
PPCL-68 cEV 1x10^9
hTERT-HPNE nEV
(i)
Blank
PANC-1 cEV
PPCL-68 cEV
hTERT-HPNE nEV
FGF2
GM-CSF
Fold change
D2
D4
(j)
Control
PANC-1 cEV
PPCL-68 cEV
Normal cell nEV
0.5 µg/mL Tunicamycin
Necrotic
Late Apoptotic
Viable
Apoptotic
24h
48h
HPDE-H6c7
hTERT-HPNE
PI
Annexin V-FITC

observing nuclei number and morphology using DAPI staining. We did not observe other signs of apoptosis in cEV treated cells, indicating that UPR/ER stress in this context is not leading to cell death (Figure S4).

Thus far, these findings confirm that cEV treatment can cause ER stress and activate the UPR in normal cells, validating our initial observation with RNA-Seq analysis. Furthermore, cEVs did not induce apoptosis, and caused an inflammatory response in treated normal cells. Taken together, these data demonstrate that cEV-mediated ER stress may be altering normal cell function, potentially a key step in the modulation of cellular phenotypes that may lead to microenvironmental remodelling conducive to disease progression.

2.4 | Pancreatic cancer cell EVs significantly alter the migratory, proliferative, and invasive capabilities of normal pancreatic epithelial cells

Our overarching hypothesis is that cEVs reprogram the cellular behaviour of normal cells upon uptake. In early preliminary studies, we observed that cEV treatment of normal cells resulted in a drastically altered morphology (data not shown). To further investigate behavioural changes induced by cEVs, we asked if cEVs altered the migratory behaviour of treated normal cells. Using a wound healing assay, we found that both PANC-1 and PPCL-68 cEVs significantly increased the migration rate of treated hTERT-HPNE or HPDE-H6c7 cells at 24h and 48h post treatment (Figure 4a-d, Videos S7-S10). Interestingly, normal cell EVs had an opposite effect, inhibiting cell migration as compared to untreated control cells. Subsequently, we sought to test if cEVs also altered the invasive potential of these normal cells. Using a Matrigel invasion assay, we found that both PANC-1 and PPCL-68 cEVs significantly increased the invasive capability of hTERT-HPNE and HPDE-H6c7 cells over 48 h (Figure 4e,f). Treatment with normal cell EVs, on the other hand, had a modest impact on treated cell invasion.

Since UPR/ER stress has been shown to impact cell proliferation (Madden et al., 2019), and the behaviour of these cells was drastically changed post-cEV treatment, we asked if cEVs altered cell proliferation. We found that cEV treatment of normal pancreatic epithelial cells significantly increased cell number, especially in hTERT-HPNE cells, potentially suggesting that the ER stress induced by cEV treatment increases cell proliferation (Figure 4g, Figure S5).

To investigate whether UPR/ER stress could mediate these behavioural changes, we performed siRNA knockdown of DDIT3 in hTERT-HPNE cells and repeated the same experiments. DDIT3 knockdown was validated using immunoblot (Figure 4h). Remarkably, we found that inhibition of DDIT3 significantly reduced the ability of hTERT-HPNE cells to invade 48 h post-cEV treatment (Figure 4i). Furthermore, DDIT3 knockdown dramatically reduced the rate of proliferation in hTERT-HPNE cells 48 h post-cEV treatment (Figure 4j). These experiments suggest that DDIT3 likely mediates increased invasive behaviour and proliferative capabilities in normal pancreas cells undergoing cEV-mediated ER stress. In the context of unchanged rates of apoptosis, these results provide evidence that activation of the UPR, specifically DDIT3, in cEV treated normal pancreas cells augments reprogramming of cell behaviour.

2.5 | Proteomics, lipidomics and metabolomics studies reveal enrichment of potential UPR/ER stress mediators in cEVs

The novel finding that cEV treated normal cells show remarkable changes in gene expression, increased proliferative, migration and invasive capabilities has striking implications on molecular changes that may eventually lead to early onset of neoplastic transformation. To better understand this phenomenon, we sought to identify potential mediators of these changes contained

FIGURE 3 cEVs induce the unfolded protein response/ER stress in treated normal pancreatic epithelial cells without increased rates of apoptosis. (a) Select known motifs identified using HOMER as significantly enriched (p-value < 0.05) in DEGs (b) Transcription Regulatory Relationships Unraveled by Sentence-based Text Mining (TRRUST) transcriptional regulatory network analysis results, predicting transcription factors responsible for regulating genes enriched in our gene set. Select results shown from HPDE-H6c7 upregulated genes. (c) Heatmap showing leading genes in the UPR/ER Stress pathways, enriched in our DEG gene set in HPDE-H6c7 (left) and hTERT-HPNE (right) cells. $N = 3$ per condition. (d) qPCR data recapitulating upregulation in key mediators of UPR/ER stress in HPDE-H6c7 cells treated with cEVs for 24 h. $N = 3$ per condition. (e) Luciferase quantification showing upregulation in binding activity of the ER stress-response element (ERSE) promoter, indicating increased UPR/ER stress in cEV treated normal cells 24 h post treatment. Tunicamycin serves as a positive control for UPR/ER stress induction. $N = 3$ per condition. (f) Immunoblots validating upregulation of key UPR/ER stress mediators 24 h post-cEV treatment. 15–20 μg of protein was loaded per lane. (g) Immunoblot demonstrating significantly increased ERN1/IRE1 and phosphorylated ERN1/IRE1 post-cEV treatment. 20 μg of protein was loaded per lane. (h) Luciferase quantification data showing upregulation in binding activity of ERSE promoter, induced by treatment with cEVs isolated using size exclusion chromatography. $N = 3$ per condition. (i) Cytokine quantification data showing upregulation of fibroblast growth factor 2 (FGF2) and granulocyte-macrophage colony-stimulating factor (GM-CSF) in the media of cEV treated normal cells treated with cEVs after 2 and 4 days. $N = 4$ per condition. (j) Flow cytometry Annexin V quantification data of HPDE-H6c7 or hTERT-HPNE cells treated with PANC-1 cEVs, PPCL-68 cEVs, the alternate normal cell EVs or Tunicamycin as a positive control. Percentages indicate the percentage of cells which are viable, undergoing apoptosis, undergoing late apoptosis (dead) or necrosis (dead). ns = $p > 0.05$, * = $p \leq 0.05$, ** = $p \leq 0.01$, *** = $p \leq 0.001$ and **** = $p \leq 0.0001$.

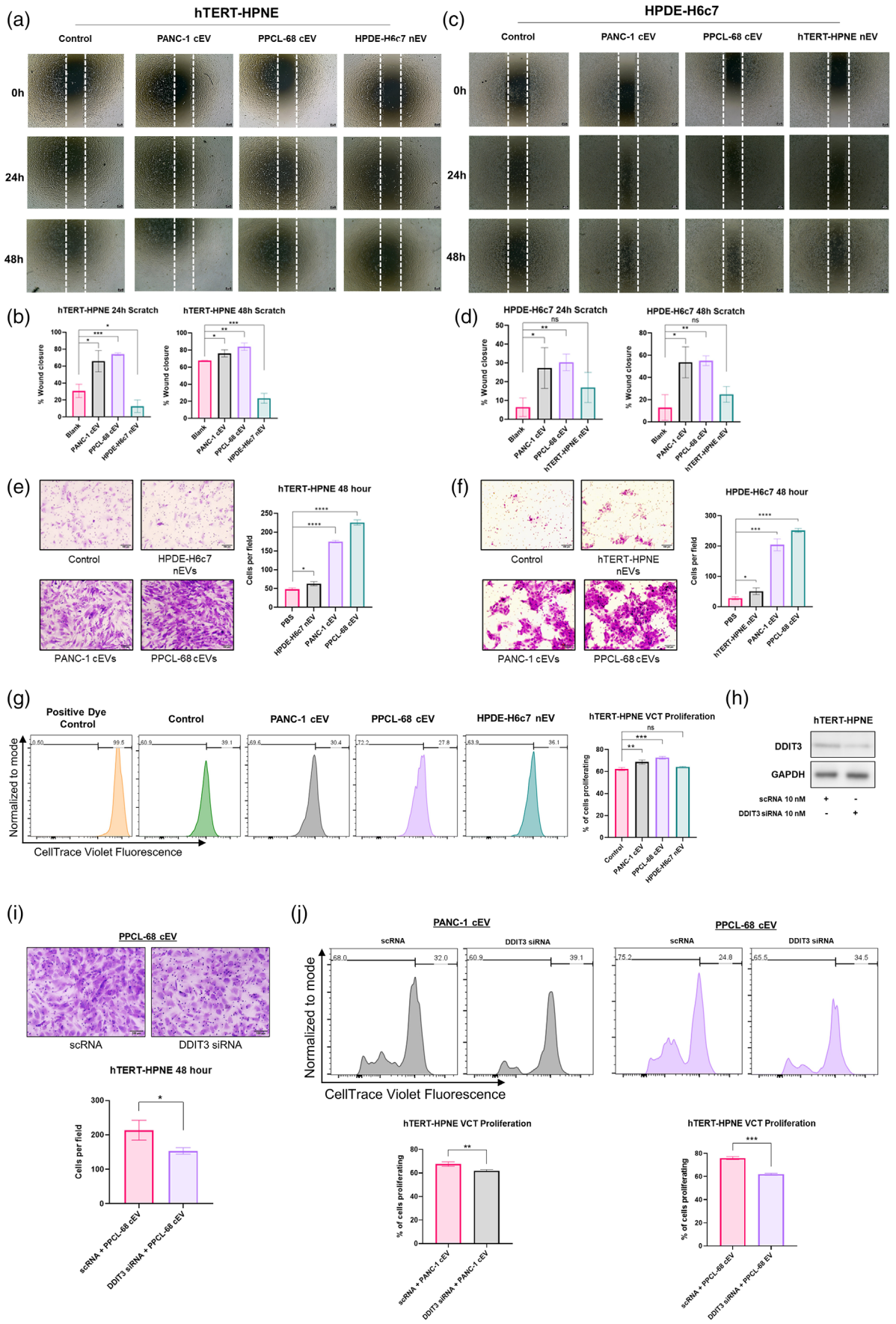
(a)
hTERT-HPNE
Control
PANC-1 cEV
PPCL-68 cEV
HPDE-H6c7 nEV
0h
24h
48h
(c)
HPDE-H6c7
Control
PANC-1 cEV
PPCL-68 cEV
hTERT-HPNE nEV
0h
24h
48h
(b)
hTERT-HPNE 24h Scratch
hTERT-HPNE 48h Scratch
% Wound closure
Blank
PANC-1 cEV
PPCL-68 cEV
HPDE-H6c7 nEV
(d)
HPDE-H6c7 24h Scratch
HPDE-H6c7 48h Scratch
% Wound closure
Blank
PANC-1 cEV
PPCL-68 cEV
hTERT-HPNE nEV
(e)
Control
HPDE-H6c7 nEVs
PANC-1 cEVs
PPCL-68 cEVs
hTERT-HPNE 48 hour
Cells per field
PBS
HPDE-H6c7 nEV
PANC-1 cEV
PPCL-68 cEV
(f)
Control
hTERT-HPNE nEVs
PANC-1 cEVs
PPCL-68 cEVs
HPDE-H6c7 48 hour
Cells per field
PBS
hTERT-HPNE nEV
PANC-1 cEV
PPCL-68 cEV
(g)
Positive Dye Control
Control
PANC-1 cEV
PPCL-68 cEV
HPDE-H6c7 nEV
Normalized to mode
CellTrace Violet Fluorescence
hTERT-HPNE VCT Proliferation
% of cells proliferating
Control
PANC-1 cEV
PPCL-68 cEV
HPDE-H6c7 nEV
(h)
hTERT-HPNE
DDIT3
GAPDH
scRNA 10 nM
DDIT3 siRNA 10 nM
(i)
PPCL-68 cEV
scRNA
DDIT3 siRNA
hTERT-HPNE 48 hour
Cells per field
scRNA + PPCL-68 cEV
DDIT3 siRNA + PPCL-68 cEV
(j)
PANC-1 cEV
scRNA
DDIT3 siRNA
PPCL-68 cEV
scRNA
DDIT3 siRNA
Normalized to mode
CellTrace Violet Fluorescence
hTERT-HPNE VCT Proliferation
% of cells proliferating
scRNA + PANC-1 cEV
DDIT3 siRNA + PANC-1 cEV
hTERT-HPNE VCT Proliferation
% of cells proliferating
scRNA + PPCL-68 cEV
DDIT3 siRNA + PPCL-68 cEV

in the EV cargo. We performed multi-omics analysis and quantification of the biomolecular content contained in cEVs derived from the six different pancreatic cancer cell lines (PANC-1, SW-1990, Capan-1, MiaPaCa-2, PPCL-68, and PPCL-46) and compared their biochemical profiles to normal cell EVs (nEVs) derived from the normal cell lines hTERT-HPNE and HPDE-H6c7 (Figure 5a). We used two independent EV isolation methods, ultracentrifugation with filtration (UC) and EVTrap, a magnetic bead-based isolation method, for proteomics profiling experiments to obviate potential protein contamination issues introduced by a given EV enrichment method. Principal Component Analysis (PCA) of proteomics and targeted metabolomics profiling revealed clear separation between cEVs and nEVs, indicating distinct protein, small molecule, and lipid profiles (Figure 5b-e). Interestingly, each approach identified an array of distinct molecules enriched in cEV cargo that could potentially mediate and/or regulate UPR/ER stress in normal epithelial cells.

Shotgun proteomics revealed 332 proteins significantly dysregulated in cEVs compared to nEVs between both ultracentrifugation and EVTrap isolation methods (Figure 6a). Of these, several of the upregulated proteins are involved in targeted protein degradation and ubiquitination, including tumour susceptibility 101 (TSG101), member RAS oncogene family (RAB40C), UBA domain containing 2 (UBAC2), cullin 5 (CUL5), RAS like proto-oncogene A (RALA), and transmembrane protein 59 (TMEM59) (Figure 6b). We validated upregulation of TSG101, TMEM59, UBAC2, RALA and RAB40C in cEVs using immunoblot (Figure 6c). We posit that cEV enrichment for these specific proteins could likely alter the normal protein degradation process, impacting protein folding and clearance functions, when internalized by normal cells.

Separately, we also performed multiple reaction monitoring (MRM)-based quantitative mass spectrometry, which included analysis of 269 polar metabolites and 1021 lipid species, that provided novel insights into potential mediators of UPR/ER stress enriched in cEV cargo. Visualization of significantly dysregulated lipids using a heatmap, confirmed differential expression patterns between cEVs and nEVs (Figure 7a). Further investigation identified enrichment of lipid species containing a palmitic acid (16:0) moiety, as well as several sphingomyelin (SM) species in cEVs (Figure 7b). Palmitic acid has been shown to induce UPR in pancreatic islet cells (Hatanaka et al., 2014; Karaskov et al., 2006) while altered sphingolipid metabolism is a contributor to the UPR (Kajiwara et al., 2012; Weston-Green et al., 2018). To investigate whether this could be occurring in our cEV treated normal cells, we treated HPDE-H6c7 ERSE luciferase reporter cells with various concentrations of palmitic acid. We found that ER stress was induced at 75 μM (Figure 7c), well below commonly reported doses of 250–500 μM and higher in other cell types (Ben-Dror & Birk, 2019; Kong et al., 2021). We confirmed upregulation of DDIT3 protein 24 h after treatment with 75 μM of palmitic acid (Figure 7d).

Ingenuity Pathway Analysis (IPA) of significantly dysregulated metabolites in cEV cargo was used to identify pathways enriched in cEVs. By analyzing the commonly dysregulated metabolites within cEVs from at least four of the six cancer cell lines tested, we found that cEVs were enriched in dysregulated metabolites involved in the citrulline biosynthesis and tRNA charging pathways (Figure 8a). This aligned with our previous STRING and RNA-Seq analysis of unique DEGs. Metabolites central to these processes, including arginine, ornithine, N-acetylornithine, glutamine, and proline, were significantly dysregulated in cEVs compared to nEVs (Data S4). As tRNA charging dysregulation was identified, in the context of activation of the UPR, we wondered whether activation of the PERK arm of the UPR could be regulating translation. PERK activation (via phosphorylation and dimerization) can lead to the phosphorylation of eIF2α, reducing translation. To investigate this, we looked at the protein expression of phosphorylated PERK (T980) and phosphorylated eIF2α (S51). Interestingly, we found that the expression of both phosphorylated PERK and phosphorylated eIF2α were elevated post-cEV treatment (Figure 8b).

On further investigation of amino acids, we found that arginine, glutamine, and proline were all significantly downregulated in cEVs compared to nEVs (Figure 8c). N-acetylornithine was also downregulated, whereas cEVs were enriched for ornithine (Data S4). We also observed enrichment of oncometabolites, such as succinate, and accumulation of phenylalanine in cEVs (Figure 8c, Data S4). We validated upregulation of ornithine, succinate, phenylalanine, and downregulation of arginine in separate MRM-mass spectrometry-based validation experiments (Figure S6).

Taken together, our data, for the first time demonstrate that cEVs are enriched for multiple classes of biomolecules which may synergistically induce UPR/ER in normal pancreatic cells that may drive some of the earliest molecular signalling changes in normal pancreatic cells.

FIGURE 4 cEVs increase the migration, invasion and proliferation of treated normal pancreas cells in a partially-DDIT3 dependent manner. (a-d) Representative images and quantifications from a wound healing scratch assay in (a-b) hTERT-HPNE or (c-d) HPDE-H6c7 cells demonstrating significant increase in the migration rate of cEV treated cells 24- and 48-h post treatment. $N = 3$ replicates per condition. (e-f) Representative images and quantifications from a Matrigel invasion assay demonstrating significantly increased invasive capability of (e) hTERT-HPNE or (f) HPDE-H6c7 cells treated with cEVs 48-h post treatment. $N = 3$ replicates per condition. (g) Proliferation analysis of hTERT-HPNE cells treated with PANC-1 cEVs, PPCL-68 cEVs, or HPDE-H6c7 nEVs 48-h post treatment, demonstrating a significantly increased percentage of cells undergoing proliferation in the cEV treated groups. $N = 3$ replicates per condition. (h) Immunoblot validating siRNA knockdown of DDIT3 at a concentration of 10 nM. (i) Representative images and quantification of a Matrigel invasion assay demonstrating the decreased invasive capability of hTERT-HPNE cells treated with PPCL-68 cEVs with DDIT3 siRNA inhibition compared to scRNA treatment. $N = 3$ replicates per group. (j) Proliferation analysis of hTERT-HPNE cells treated with either PANC-1 or PPCL-68 cEVs, demonstrating a reduced percentage of cells undergoing proliferation with DDIT3 siRNA knockdown compared to scRNA treatment. $N = 3$ replicates per group. ns = $p > 0.05$, * = $p \leq 0.05$, ** = $p \leq 0.01$, *** = $p \leq 0.001$ and **** = $p \leq 0.0001$.

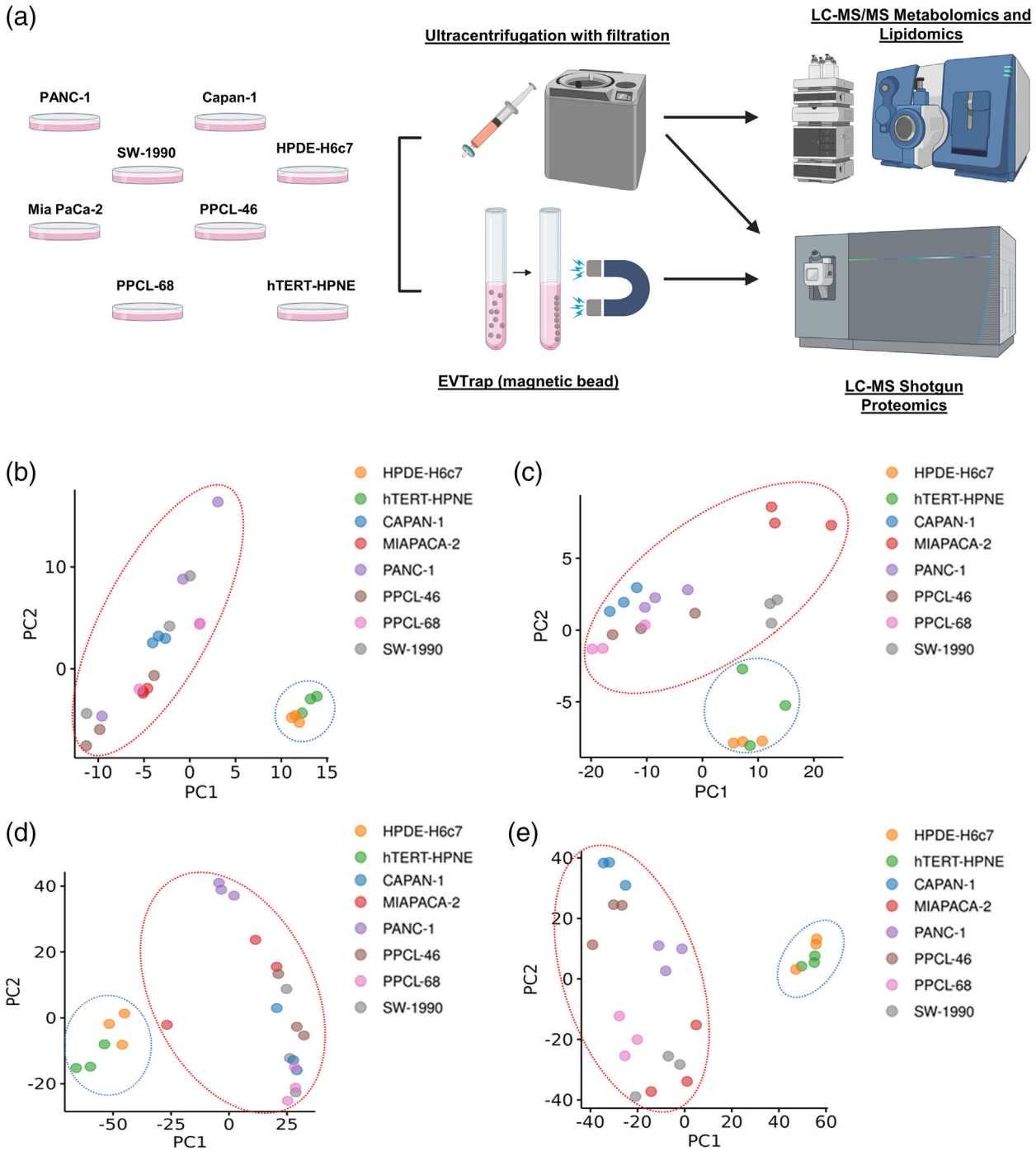

FIGURE 5 Multi-omics analysis of cEVs and nEVs reveals enrichment in potential regulators of UPR/ER stress. (a) Experimental protocol for EV isolation from six pancreatic cancer cell line (cEV) and two normal pancreas cell line (nEV) models. Proteomics was performed on EVs isolated using two independent methods, ultracentrifugation and EVTrap. (b-e) Principal component analysis (PCA) plots of (b) polar metabolites (c) lipids and (d) proteins isolated by EVTrap and (e) proteins isolated by ultracentrifugation, in cEVs and nEVs. Red circles encompass cEV samples, blue circles encompass nEV samples. $N = 3$ independent EV isolations per cell line.

3 | DISCUSSION

While pancreatic cancer cell derived EVs (cEVs) are thought to regulate intercellular communication and signal transduction leading to proliferation, invasion and metastasis, a deeper understanding of how these events are mediated is critical to understand disease aetiology. How specific molecular signalling events, triggered upon cEV internalization by normal cells, impact the

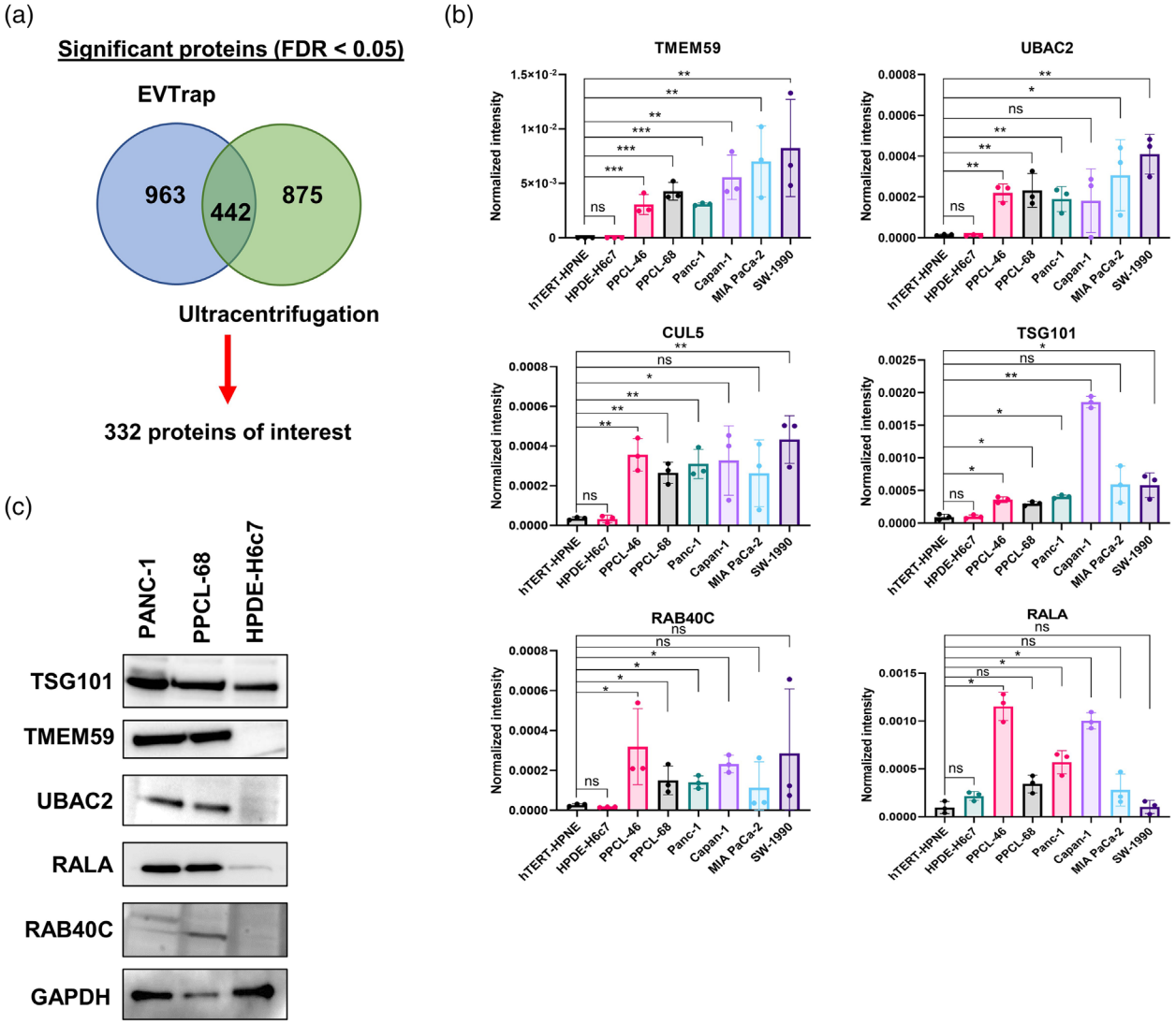

FIGURE 6 Shotgun proteomics reveals potential mediators of UPR/ER stress enriched in cEVs. (a) Venn diagram showing number of significantly dysregulated proteins identified by either EVTrap or ultracentrifugation EV isolation methods. The total number of proteins yielded 332 proteins of interest, defined as FDR-adjusted p-value < 0.05, Fold change > 3 or < 0.5, and a matching expression trend (either upregulated or downregulated) in each isolation method (EVTrap and ultracentrifugation). (b) Select proteins involved in the regulation of protein transport and ubiquitination, as defined by gene ontology analysis and literature search, which were enriched in cEVs. Values are plotted as means with standard deviation. Representative intensity data from EV samples isolated by ultracentrifugation. $N = 3$ independent EV isolations per cell line. (c) Immunoblot validations of TSG101, TMEM59, UBAC2, RALA and RAB40C from proteomics data. Images captured from independent EV isolations from each cell line. 15 μg of EV protein was loaded per lane. ns = $p > 0.05$, * = $p \leq 0.05$, ** = $p \leq 0.01$, and *** = $p \leq 0.001$.

function of those normal cells remains understudied. Especially in the context of pancreatic cancer, understanding key changes within non-cancerous cells that shape the microenvironment is critical toward designing novel therapeutic interventions and diagnostics. In this study, using an array of human established and PDX PDAC and normal pancreas cell line models, we have demonstrated that pancreatic cancer cEVs drastically alter the behaviour and gene expression profiles of treated normal pancreatic cells. These changes are dramatic, and our findings elucidate a new perspective for understanding pancreas cancer onset and progression.

Specifically, our data show that cEVs cause ER stress and activate the unfolded protein response (UPR) in treated cells. Subsequently, this leads to an inflammatory response and drives increased proliferation, invasion, and enhanced migration. Furthermore, we demonstrate that cEVs are enriched for an array of molecular mediators of ER stress and the UPR, including protein homeostasis regulators, oncometabolites and palmitic acid. Finally, we demonstrate that the UPR mediator DDIT3 positively regulates the proliferation and invasive potential of cEV treated normal cells.

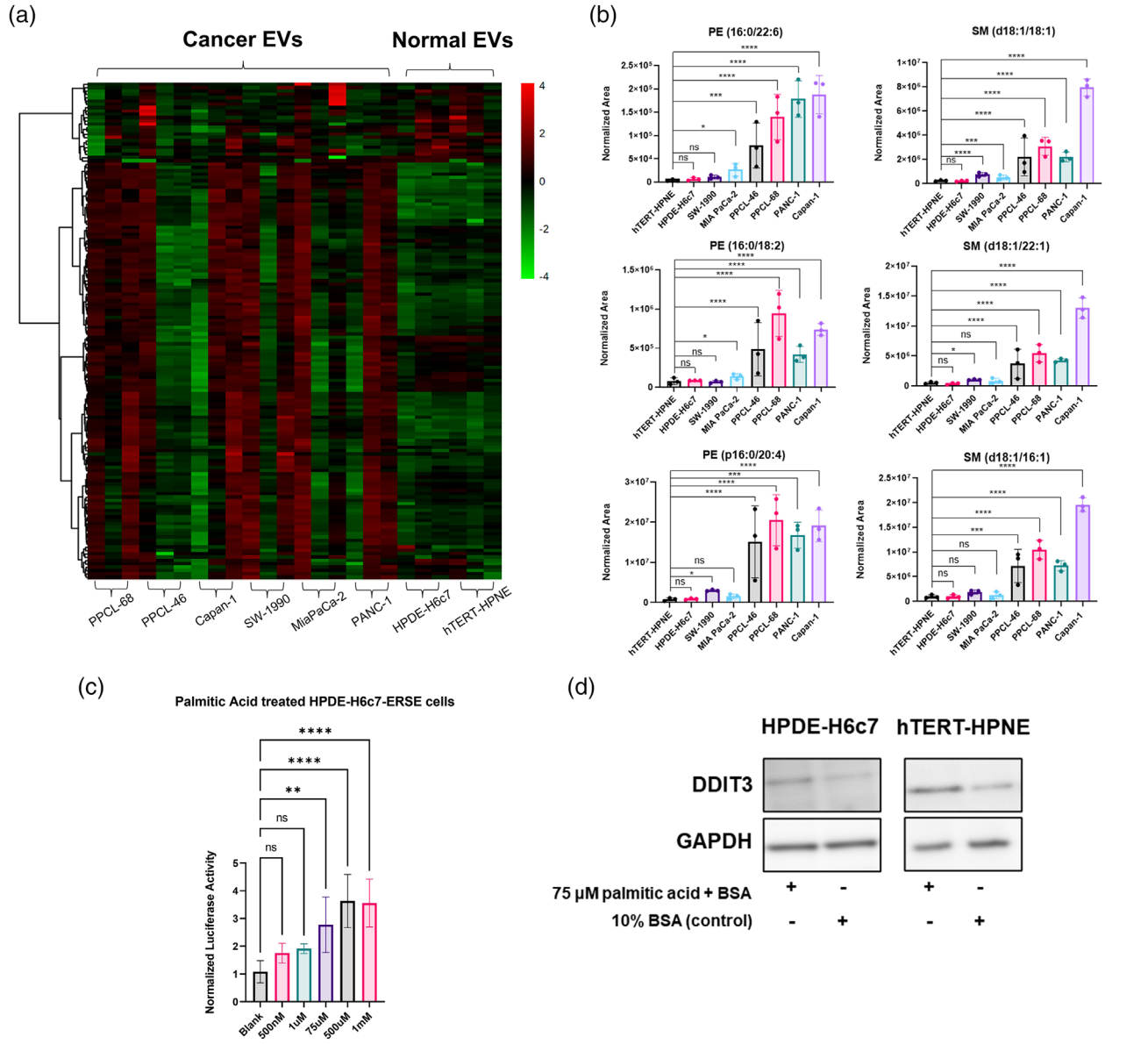

FIGURE 7 cEVs and nEVs have distinct lipid profiles. (a) Heatmap depicting distinct lipid expression profiles in cEVs compared to nEVs, as determined by LC-MS/MS. (b) Select lipid species containing palmitic acid (16:0) and SM lipid species which were significantly upregulated in cEVs. Means with standard deviation are plotted. $N = 3$ independent EV isolations per cell line. (c) ERSE-luciferase activity plotted from HPDE-H6c7 cells treated with various concentrations of palmitic acid esterified to bovine serum albumin (BSA). Means with standard deviation are plotted. $N = 5$ per condition. (d) Immunoblot demonstrating elevated levels of DDIT3 in both hTERT-HPNE and HPDE-H6c7 cells with palmitic acid treatment compared to BSA. ns = $p > 0.05$, * = $p \leq 0.05$, ** = $p \leq 0.01$, and *** = $p \leq 0.001$.

The endoplasmic reticulum is crucial for protein maturation and proper folding, with approximately 30% of all proteins undergoing ER processing (Clarke et al., 2012; Hetz, 2012). If this intricate process is disrupted, inducing ER stress, cells respond with coping mechanisms that include the UPR (Hetz, 2012). Canonically under sustained ER-stress, apoptosis is triggered leading to cell clearance (Hetz & Papa, 2018). Our data suggest that all three arms of the UPR may initially be activated upon cEV treatment, as we observed increased expression of various intermediaries such as DDIT3, XBP1 (both the spliced and unspliced variant), EIF2AK3/PERK and ATF6. Unconventional splicing of XBP1 to generate the spliced protein form creates the active transcription factor to efficiently activate the UPR (Yoshida et al., 2001). This multi-pronged activation may also partially explain why we observe unexpected changes within cEV treated cells, such as decreased lipogenesis or protein folding as suggested by the GO analysis of our RNA-Seq experiment. Lipogenesis and protein folding are often increased during the UPR (Basseri & Austin, 2012; Moncan et al., 2021; Zheng, 2010). It is possible that abrogated protein folding may be causal, rather than responsive, in this study as cEVs are enriched for several proteins responsible for managing protein trafficking and processing. Given these cells

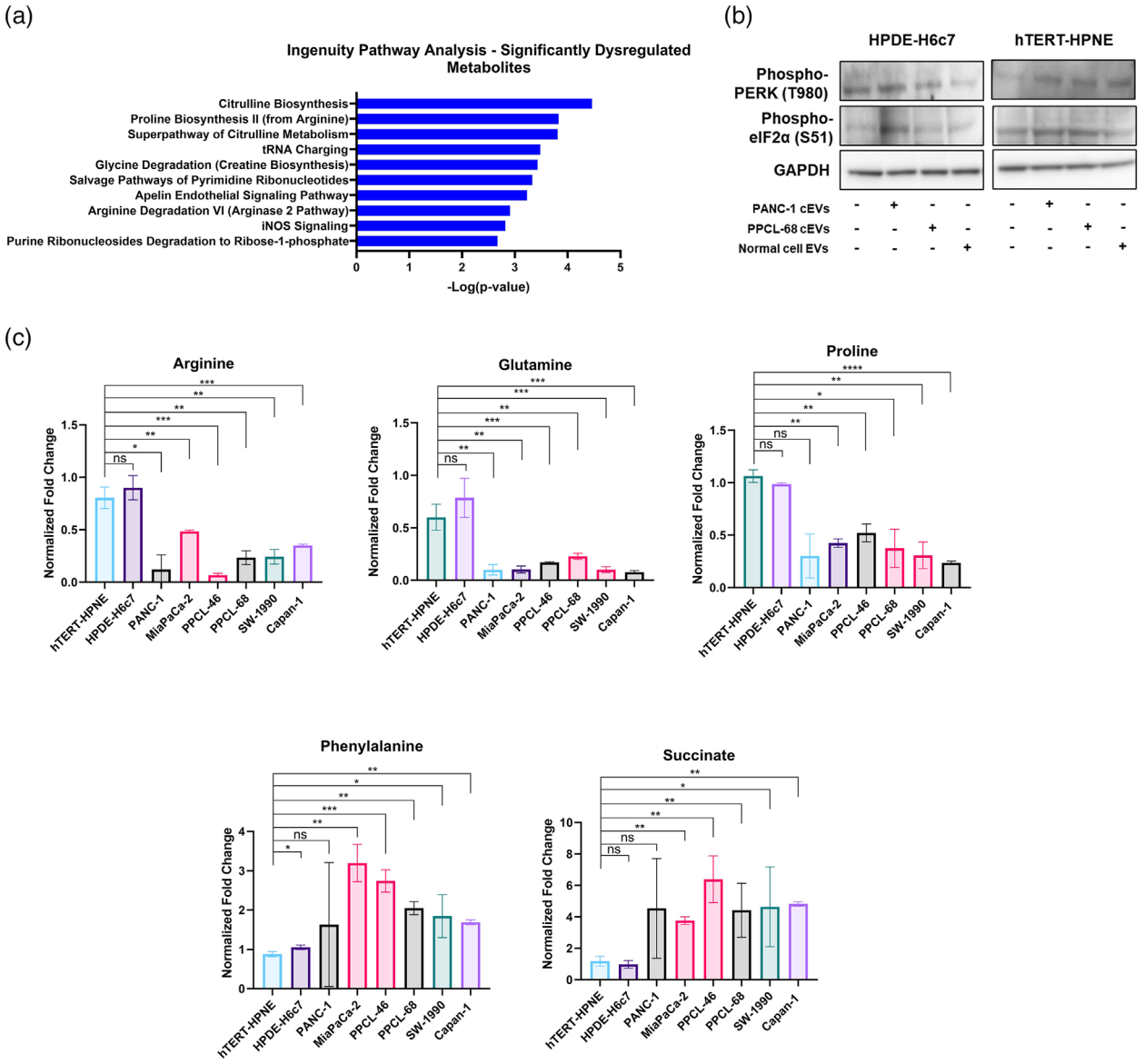

FIGURE 8 cEVs are enriched for oncometabolites and molecules which alter tRNA aminoacylation in treated normal pancreas cells. (a) Ingenuity pathway analysis (IPA) identified significant dysregulation in metabolites related to citrulline biosynthetic pathways and tRNA charging in cEVs compared to nEVs. FDR-adjusted $p < 0.05$ was used to select significant pathways and -log (p-value) was used for visualization. (b) Immunoblot measuring expression of phosphorylated eIF2α and phosphorylated PERK in HPDE-H6c7 and hTERT-HPNE cells treated with PANC-1 cEVs, PPCL-68 cEVs or normal cell nEVs 24 h post treatment. (c) Levels of arginine, glutamine, proline, phenylalanine, and succinate in cEVs and nEVs as determined by LC-MS/MS. Means with standard deviations are plotted. $N = 3$ independent EV isolations per condition. ns = $p > 0.05$, * = $p \leq 0.05$, ** = $p \leq 0.01$, *** = $p \leq 0.001$ and **** = $p \leq 0.0001$.

are not undergoing apoptosis, and we observe dramatic behavioural changes, it is not surprising that we may have identified non-canonical responses to ER stress in cEV treated cells.

Importantly, without increased rates of apoptosis and with increased proliferation of cEV treated cells in a DDIT3 dependent manner, this suggests a possible survival mechanism is activated in these cells. One consideration is that in this study, the normal cell models employed are immortalized established cell lines. In some ways, this may imbue certain propensities for these cells to respond differently to elevated DDIT3 than primary normal cells would. This may also explain the unique changes we identify in hTERT-HPNE or HPDE-H6c7 cells. Though they are closely related and non-tumourigenic, they represent different types of "normal" pancreas cells. Interestingly, DDIT3 has been shown to inhibit apoptosis in certain contexts, particularly in neuronal cells (Gow & Wrabetz, 2009; Halterman et al., 2010). DDIT3 has also demonstrated an ability to regulate cell behaviour in hepatocellular carcinoma and breast cancer cells (Guan et al., 2020; Xiao et al., 2021). Nonetheless, these changes are dramatic in the context of expected normal cell behaviour, and thus warrant further investigation as mediators of disease progression.

Given the fundamental role of the UPR in normal physiology, abnormal ER stress has also been implicated across an array of pathologies including cancer. IRE1α is the fifth-most mutated kinase in cancer and the UPR has been shown to impact many cancer hallmarks, including angiogenesis, genome stability, inflammation, metastasis, and drug resistance (Cubillos-Ruiz et al., 2017;

Urra et al., 2016). Specific to the pancreas, UPR is constitutively active due to high demand for protein synthesis and maintenance of acinar cell homeostasis (Hess et al., 2011). However, prolonged UPR can lead to inflammation and as such, UPR is a driver in chronic pancreatitis and diabetes (Riahi et al., 2018; Sah et al., 2014). Our data demonstrate that cEVs induce an inflammatory response, with upregulation of both FGF2 and GM-CSF. ER stress further mediates the progression of pancreatic intraepithelial neoplasia (PanIN) to pancreatic ductal adenocarcinoma (PDAC) through expression of anterior gradient-2 (AGR2) (Dumartin et al., 2017).

Framing our findings within the context of these previous reports, it is possible that in the earliest stages of PDAC development, cancer cells release EVs which are internalized by neighbouring normal cells, inducing ER stress, promoting inflammation and disease progression.

As we continue to investigate potential mediators of these signalling changes, it seems clear that analysing multiple classes of EV biomolecules is important. Each of our analyses identified potential inducers of ER stress. Our proteomics analysis of EVs indicated significant enrichment of proteins which are integrally involved with protein trafficking and degradation. One interesting finding was that TSG101 is enriched in pancreatic cEVs; TSG101 is widely used as a marker for demonstrating enrichment of EVs generally, given its association with the endosomal sorting complex required for transport (ESCRT) pathway (Willms et al., 2016). Though TSG101 functions in the biogenesis of multivesicular bodies (MVBs), the functional consequences of enrichment in our cEVs, and EVs more broadly, remains unknown. Functional inactivation of TSG101 in mouse fibroblasts resulted in increased EGFR recycling, leading to prolonged EGF-stimulated activation of Mitogen-activated protein kinase 3 (MAPK3)/Extracellular Signal-Regulated Kinase 1 (ERK1) and Mitogen-activated protein kinase 1 (MAPK1)/Extracellular Signal-Regulated Kinase 2 (ERK2) (Babst et al., 2000; Katzmann et al., 2002). Interestingly, a recent study demonstrated that Angiogenic Factor with G-Patch and FHA Domains 1 (AGGF1)-dependent inactivation of MAPK3/ERK1 and MAPK1/ERK2 may mediate ER stress in cardiac tissue (Yao et al., 2017). It is therefore possible that TSG101 enrichment in cEVs could alter MAPK3/ERK1 and MAPK1/ERK2 signalling in treated normal cells, leading to activation of ER stress.

Understanding lipid heterogeneity within EV subpopulations could prove critical toward understanding internalization mechanisms and signalling events which may not be captured by more commonly used proteomic and nucleic acid characterization techniques (Record et al., 2018; Tkach & Théry, 2016). We found that cEVs were enriched for lipid species esterified to a palmitic acid (16:0) moiety. Palmitic acid can induce UPR in pancreatic islet cells (Danino et al., 2015; Hatanaka et al., 2014; Karaskov et al., 2006). We have directly demonstrated that palmitic acid can induce ER stress in normal pancreatic cells at a concentration of 75 μM, to our knowledge, the lowest reported dose and relevant to the concentration we have previously quantified within cEVs (unpublished data). We further found that cEVs were enriched for SM lipids. The ER requires complex sphingolipids for homeostasis and altered sphingolipid metabolism has shown to be a contributor to UPR (Kajiwara et al., 2012; Weston-Green et al., 2018). A sudden shock of SM species into cEV treated normal cells may alter sphingolipid homeostasis, producing the necessary conditions for ER stress and UPR activation.

Metabolomic analysis of EVs in this study has augmented the discovery of potential metabolic mediators of cancer progression (Clos-Garcia et al., 2018; Tao et al., 2019; Williams et al., 2019). For example, EV polar metabolite analysis identified involvement of biosynthesis pathways which interface with UPR/ER stress. tRNA charging was identified as a significantly dysregulated pathway in our metabolomics analysis. This aligned with findings from our protein-protein interaction STRING analysis, which indicated gene expression alterations related to tRNA-aminoacylation. This is striking, as abrogated tRNA-aminoacylation has been linked to induction of ER stress and subsequent activation of the UPR (Castranova et al., 2016). Given that cEVs are enriched in multiple biomolecular classes, which directly, or potentially indirectly, regulate ER stress and protein homeostasis, there could be a synergistic effect across biomolecular classes. The extent to which EVs containing various micro-RNA and other RNA species have been implicated in cancer also needs to be delineated in future studies.

Our ongoing studies are investigating these potential mechanisms and how the induction of UPR/ER stress in cEV treated non-tumourigenic pancreatic cells impacts their function in the long-term. These studies may prove critical toward understanding potential molecular drivers of normal cell alteration at the earliest stages of PDAC development.

4 | MATERIALS AND METHODS

4.1 | Cell culture

PDAC cell lines PANC-1 (CRL-1469), Capan-1 (HTB-79), SW-1990 (CRL-2172), MiaPaCa-2 (CRM-CRL-1420) were purchased from American Type Culture Collection (ATCC) and grown in modified MEM (Gibco, #A1048801) with 10% HI-FBS (Gibco, #10082147) and 1% Penicillin-Streptomycin (Gibco, #15140122). The normal pancreatic epithelial cell line hTERT-HPNE (CRL-4023) was also purchased from ATCC and HPDE-H6c7 (ECA001-FP) cells were purchased from Kerafast and grown in keratinocyte serum-free media supplemented with bovine pituitary extract and recombinant epidermal growth factor (Gibco, #37010022) with 1% Penicillin-Streptomycin. The patient-derived xenograft PDAC cell lines PPCL-68 and PPCL-46 were generated as previously described (Pham et al., 2016) and cultured in advanced MEM (Gibco, #12492013) with 5 mM L-Glutamine

(Gibco, #25030081), 10% HI-FBS and 1% Penicillin-Streptomycin. All cells were grown in a 5% CO_2 incubator at 37°C. All cell lines were authenticated and tested by DNA fingerprinting short tandem repeat analysis (STR) at the Lombardi Comprehensive Cancer Center Tissue Culture and Shared Resource. Testing for mycoplasma and contaminants were negative for all cell lines used.

4.1.1 | DDIT3 siRNA treatment

ON-TARGETplus SMARTPool siRNA targeting human DDIT3 (#L-004819-00-0005) and a scrambled control siRNA (#D-001810-10-05) were purchased from Horizon Discovery. Cells were seeded and siRNA was transfected using PepMute siRNA Transfection Reagent (SignaGen Laboratories, # SL100566) according to manufacturer's protocol. After 24–48h post-transfection, cells were detached with trypsin and used for downstream experiments.

4.2 | EV isolation from conditioned media and characterization

We have submitted all relevant data of our experiments to the EV-TRACK knowledgebase (EV-TRACK ID: EV210204) (Van Deun et al., 2017). cEVs were isolated from six PDAC cancer cell lines (PANC-1, MiaPaCa-2, Capan-1, SW-1990, PPCL-46 and PPCL-68) and two normal pancreatic cell lines (hTERT-HPNE and HPDE-H6c7). EV preparations were characterized using immunoblot, nanoparticle tracking analysis and cryogenic electron microscopy (methods below). We also developed a SMAD2/3/4-response element-luciferase reporter system stably expressed in a fibroblast cell line to measure the biological activity of cEV isolations (Figure S7, methods below). Once biological activity was confirmed, EVs were used for downstream experiments.

4.2.1 | EV isolation cell culture conditions

When cells were ∼50 - 60% confluent, media was changed to the cells respective base media containing 10% exosome depleted FBS (Gibco, A2720801) instead of 10% HI-FBS. For normal cells, no FBS was added, and media was changed to fresh serum free media. Cells were grown for an additional 48 h to make conditioned media. EVs were isolated from conditioned media using either differential ultracentrifugation with filtration (UC), a magnetic bead-based method, EVTrap (EVT) or size exclusion chromatography with filtration (SEC).

4.2.2 | Ultracentrifugation

Conditioned media was collected from tissue culture flasks and moved to sterile 50 ml conical tubes. Samples were spun at 1600 x g for 20 min, at 4°C. Samples were then transferred by inversion to fresh ultracentrifuge tubes (Beckman, #326823) and placed in a SW-28 (Beckman) rotor. Tubes were then spun at 10,000 x g for 20 min at 4°C in an ultracentrifuge (Beckman, L8-70M). The supernatant was filtered using 0.2 μM syringe filters (Millipore Sigma, #SLGP033RB) into new ultracentrifuge tubes. Samples were placed back in a SW-28 rotor and spun at 120,000 x g for 70 min, at 4°C. Supernatant was removed from tubes by inversion and the final EV pellet was re-suspended in 50 μl 1 X DPBS. Samples were stored at −80°C until further processing.

4.2.3 | Size exclusion chromatography

Conditioned media was collected from tissue culture flasks and moved to sterile 50 ml conical tubes. Samples were spun at 2500 x g for 10 min at 25°C. Supernatants were next transferred to clean 50 ml conical tubes and again spun at 2500 x g for 10 min at 25°C. Samples were then filtered and concentrated using 100 kDa centrifugal filters (Pall Corporation, #OD100C65). Samples were spun at 3000 x g for 30 min at 25°C. Flow through was discarded and the remaining supernatant was added to filters. Samples were again spun at 3000 x g for 30 min at 25°C. This was repeated until all supernatant was filtered/concentrated. Next, concentrated media was collected and further filtered using 15 ml Amicon 100 kDa filters (Millipore Sigma, #UFC9100) by spinning at 3000 x g for 20 min at 25°C. EVs were subsequently isolated from the final concentrated media using 70 nM SEC columns (IZON, qEV2, #SP4) using an automated fraction collector, according to manufacturer's protocol. Fractions were stored at −80°C. Fractions containing EVs (F1-F3) were lyophilized, resuspended in 1 x DPBS, and combined to make a working stock solution of EVs.

4.2.4 | EVTrap

Conditioned media was collected from tissue culture flasks and moved to sterile 50 ml conical tubes. Samples were spun at 1600 x g for 20 min at 25°C. Supernatant was transferred to clean 15 ml tubes. Next, media loading buffer was added to the tubes, and samples were mixed by inversion. Magnetic EVtrap beads (Wu et al., 2018) were then added to samples and tubes were incubated for 1 h with end-over-end rotation at 25°C. Tubes were then placed on a magnetic separator and solution was removed. Beads were washed with media loading buffer, followed by two washes with 1 x DPBS. EVs were eluted from beads using 100 mM triethylamine (TEA) by incubation with rigorous shaking at room temperature for 10 min. EVs were collected, samples were lyophilized and re-suspended in 1 x DPBS. Samples were then stored at −80°C until further use.

4.3 | EV protein marker immunoblot

To investigate the expression of EV-associated proteins, we measured the protein levels of CD63, CD81, TSG101, EpCAM, ALIX, ANXA5, FLOT1, GM130 and ICAM by immunoblot using the Exo-Check Exosome Antibody Array (System Biosciences, #EXO-RAY210A). Protein concentration for EV samples was measured using BCA (Thermo Fisher, #23225) and 30 μg of protein was analysed according to manufacturer's protocol.

4.4 | Nanoparticle Tracking Analysis (NTA)

NTA was accomplished using a NanoSight NS300 (Malvern Panalytical) equipped with a high sensitivity sCMOS camera, 531 nm laser and automatic syringe pump. 1 μL of EVs resuspended in 1x PBS was diluted to a final volume of 1 ml with 1x PBS prior to being loaded on the automatic syringe injector. Camera and detection settings can be found in Data S5. Videos were captured and processed using NTA 3.3 Dev Build 3.3.104 with three videos of 30 s per measurement, per sample. Concentrations as determined by NTA were used for downstream experiments.

4.5 | Cryogenic electron microscopy

EV samples resuspended in 1x DPBS were frozen at −80°C and shipped on dry ice to the Molecular Electron Microscopy Core at the University of Virginia. An aliquot of sample (~3.5 μl) was applied to a glow-discharged, perforated carbon-coated grid (2/1-3C C-Flat; Protochips, Raleigh, NC), manually blotted with filter paper, and rapidly plunged into liquid ethane. The grids were stored in liquid nitrogen, then transferred to a Gatan 626 cryo-specimen holder (Gatan, Warrrendale, PA) and maintained at ~180°C. Low-dose images were collected at a nominal magnification of 29,000X on a Tecnai F20 Twin transmission electron microscope (ThermoFisher Scientific, Hillsboro, OR) operating at 120 kV. The digital micrographs were recorded on a Gatan US4000 CCD or a Teitz XF416 camera.

4.6 | RNA-sequencing

RNA was isolated from cells using the RNeasy Mini Kit (Qiagen, #74104) according to the manufacturers protocol. Library construction and sequencing was performed by Novogene Corporation (Sacramento, CA). RNA quality control (QC) was assessed using Qubit (Thermo Fisher) and Bioanalyzer (Agilent) analysis. Libraries were prepared using NEBNext Ultra II non-directional RNA Library Prep kit (New England BioLabs, # E7770S). Library quality and concentration was assessed with Labchip and qPCR. Libraries were sequenced on a Novaseq6000 (Illumina) using PE150 sequencing at a depth of 30 million reads. Downstream analysis was performed using STAR, HTSeq, Cufflink and custom scripts. Reference genome and gene model annotation files were downloaded directly from NCBI and paired-end clean reads were aligned using STAR (v2.5). Fragments Per Kilobase Million (FPKM) counts for each gene were calculated based on the length of the gene and read counts mapped to that gene.

4.7 | Mass spectrometry solvents and standards

All solvents, including high purity formic acid (#A117-50), dichloromethane (#EW-88016-02), chloroform (#EW-80044-89), acetonitrile (#A955-4), methanol (#A456-4), isopropyl alcohol (#A461-4), and water (#W6-4) were LC-MS grade and purchased from Fisher Scientific. Debrisoquine (# D1306100MG) and taurine-d4 (#703443-100mg) were purchased from Sigma-Aldrich.

4.7.1 | Polar metabolite profiling

1. Sample preparation: 50 μl of EVs were transferred to glass tubes for extraction. 0.9 ml of water was added to each tube and samples were incubated on ice for 10 min. Next, 2 ml of methanol and 0.9 ml of dichloromethane (DCM) was added to each sample and tubes were mixed gently, but thoroughly, for 5 s. Samples were then incubated at room temperature for 30 min. Next, 1 ml of water and 2 ml of chloroform was added to each sample. Tubes were then spun at 2000 x g for 20 min at room temperature. The upper aqueous layer was collected and stored at −80°C for 5 h. Samples were then lyophilized and re-suspended in 0.2 ml of a 1:1 mixture of acetonitrile and water containing 200 ng/ml of debrisoquine (internal standard for positive mode) and 200 ng/ml of taurine-d4 (internal standard for negative mode). Samples were centrifuged and transferred to mass spectrometry glass vials just prior to data acquisition.
2. Data acquisition: 5 μl of sample was injected onto a Kinetex 2.6 μm 100 Å 100 × 2.1 mm (Phenomenex, #00A-4723-AN) using a SIL-30 AC auto sampler (Shimazdu) connected with a high flow LC-30AD solvent delivery unit (Shimazdu) and CBM-20A communication bus module (Shimazdu) online with a QTRAP 5500 (Sciex) operating in positive and negative ion mode. Samples were resolved at a 0.2 ml/min flow rate starting with 100% of solvent A holding for 2.1 min and moving to 5% of solvent A over 12 min, holding for 1 min before equilibrating to initial conditions over a period of 7 min. Auto sampler temperature was 15°C and oven temperature was 30°C. A binary solvent comprising of water (with 0.2% formic acid) and acetonitrile (with 0.2% formic acid) was used. Full gradient and MRM transitions that were used for quantitation are detailed in Data S6. The data were normalized to internal standard area and processed using MultiQuant 3.0.3 (Sciex). Source and gas settings for the mass spectrometer were as follows: curtain gas = 35, CAD gas = Medium, Ion Spray Voltage = 2500 V in positive mode and −4500 V in negative mode, temperature = 400°C, nebulizing gas = 60 and heater gas = 70.
3. Metabolite validations using multiple reaction monitoring-mass spectrometry (MRM-MS): this method was designed to measure palmitic acid (Sigma, #P0500), succinate (Sigma, #398055), uracil (Sigma, #U0750), ureidopropionic acid (Sigma, #94295), ornithine (Sigma, #W419001), phenyl-acetyl-l-glutamine (Sigma, #SMB00962), citrulline (Sigma, #C7629), arginine (Sigma, #A5006), and phenylalanine (Sigma, #P2126) using the QTRAP 5500 system. For calibration curves, twelve concentration points were used ranging from 1 ng/ml to 2500 ng/ml. LC-MS conditions were the same as above. For sample preparation, 25 μL of EV samples were combined with 40 μL of 35% water, 25% methanol and 40% isopropyl alcohol. Samples were plunged into dry ice for 30 s and heat shocked by plunging into a 37°C water bath for 90 s. This was repeated for a total of three times. Samples were then sonicated for 30 s. Next, 200 μL of methanol containing 200 ng/ml of debrisoquine and 200 ng/ml of taurine-d4 was added to samples. Tubes were vortexed for 30 s, incubated on ice for 20 min and incubated at −20°C for 20 min. Finally, samples were centrifuged at 13,000 x g for 20 min at 4°C. Supernatant was transferred to MS vials for LC-MS analysis.

4.7.2 | Lipidomics profiling

1. Sample preparation: 50 μl of EVs were lysed as described above, using the heat shock method. After sonication for 30 s, 100 μl of ice-cold isopropyl alcohol containing lipid internal standards (full list in Data S6) was added to samples. Samples were vortexed for 1 min and incubated on ice for 30 min. Finally, samples were incubated at −20°C for 2 h to complete protein precipitation, spun at 13,000 x g for 20 min at 4°C and supernatant was transferred to MS vials for LC-MS analysis.
2. Data acquisition: 5 μl of sample was injected onto an Xbridge Amide 3.5μm, 4.6×100 mm column (Waters Corporation, #186004868) using a SIL-30 AC auto sampler connected to a high flow LC-30AD solvent delivery unit and CBM-20A communication bus module online with a QTRAP 5500. A binary solvent comprising of acetonitrile and water (95:5) with 10 mM ammonium acetate as solvent A and 50:50 acetonitrile and water with 10 mM ammonium acetate as solvent B was used for resolution. Lipids were resolved at 0.7 ml/min flow rate with initial gradient at 100% of solvent A, shifting towards 99.9% solvent A over 4 min. Finally, the gradient washed with 100% of solvent B for 6 min and equilibrated to initial conditions of the remaining 6 min. Full gradient and MRM transitions can be found in Data S6. Data were normalized to internal standard area and processed using MultiQuant 3.0.3. Source and gas settings were as follows: curtain gas = 30, CAD gas = Medium, Ion Spray Voltage = 5.5 kV in positive mode and −4.5 kV in negative mode, temperature = 550°C, nebulizing gas = 50 and heater gas = 60.

4.7.3 | Proteomics profiling of EVs

1. Sample preparation: 50 μl of EVs were dried by lyophilization. Samples were then lysed to extract proteins using the phase-transfer surfactant (PTS) aided procedure (Wu et al., 2018). Proteins were reduced and alkylated by incubation in 10 mM TCEP and 40 mM CAA for 10 min at 95°C. Samples were next diluted fivefold with 50 mM triethylammonium bicarbonate and

digested with Lys-C (Wako) at 1:100 (wt/wt) enzyme-to-protein ratio for 3 h at 37°C. Trypsin was added to a final 1:50 (wt/wt) enzyme-to-protein ratio for overnight digestion at 37°C. To remove the PTS surfactants from the samples, the samples were acidified with trifluoroacetic acid (TFA) to a final concentration of 1% TFA, and ethyl acetate solution was added at 1:1 ratio. The mixture was vortexed for 2 min and then centrifuged at 16,000 × g for 2 min to obtain aqueous and organic phases. The organic phase (top layer) was removed, and the aqueous phase was collected. This step was repeated once more. The samples were dried in a vacuum centrifuge and desalted using Top-Tip C18 tips (Glygen) according to manufacturer's instructions. The samples were dried completely in a vacuum centrifuge and stored at −80°C.

2. LC-MS/MS Analysis: 20% (~1 μg) of each dried peptide sample was dissolved in 10.5 μl of 0.05% trifluoroacetic acid with 3% (vol/vol) acetonitrile containing spiked-in indexed Retention Time Standard containing 11 artificially synthetic peptides (Biognosys). The spiked-in 11-peptides standard mixture was used to account for any variation in retention times and to normalize abundance levels among samples. 10 μl of each sample was injected into an Ultimate 3000 nano UHPLC system (Thermo Fisher Scientific). Peptides were captured on a 2-cm Acclaim PepMap trap column and separated on a heated 50-cm Acclaim PepMap column (Thermo Fisher Scientific) containing C18 resin. The mobile phase buffer consisted of 0.1% formic acid in ultrapure water (buffer A) with an eluting buffer of 0.1% formic acid in 80% (vol/vol) acetonitrile (buffer B) run with a linear 60-min gradient of 6–30% buffer B at flow rate of 300 nL/min. The UHPLC was coupled online with a Q-Exactive HF-X mass spectrometer (Thermo Fisher Scientific). The mass spectrometer was operated in the data-dependent mode, in which a full-scan MS (from m/z 375 to 1500 with the resolution of 60,000) was followed by MS/MS of the 15 most intense ions (30,000 resolution; normalized collision energy - 28%; automatic gain control target (AGC) - 2E4, maximum injection time - 200 ms; 60sec exclusion].
3. Proteomics data processing: Raw data files were searched directly against the human Swiss-Prot database updated on July 16, 2019 with no redundant entries, using Byonic (Protein Metrics) and Sequest search engines loaded into Proteome Discoverer 2.3 software (Thermo Fisher Scientific). MS1 precursor mass tolerance was set at 10 ppm, and MS2 tolerance was set at 20 ppm. Search criteria included a static carbamidomethylation of cysteines (+57.0214 Da), and variable modifications of oxidation (+15.9949 Da) on methionine residues and acetylation (+42.011 Da) at N terminus of proteins. Search was performed with full trypsin/P digestion and allowed a maximum of two missed cleavages on the peptides analysed from the sequence database. The false-discovery rates of proteins and peptides were set at 0.01. All protein and peptide identifications were grouped, and any redundant entries were removed. Only unique peptides and unique master proteins were reported.
4. Label-free quantitation: All data were quantified using the label-free quantitation node of Precursor Ions Quantifier through the Proteome Discoverer v2.3 (Thermo Fisher Scientific). For the quantification of proteomic data, the intensities of peptides were extracted with initial precursor mass tolerance set at 10 ppm, minimum number of isotope peaks as 2, maximum ΔRT of isotope pattern multiplets – 0.2 min, PSM confidence FDR of 0.01, with hypothesis test of ANOVA, maximum RT shift of 5 min, pairwise ratio-based ratio calculation, and 100 as the maximum allowed fold change. The abundance levels of all peptides and proteins were normalized to the spiked-in internal iRT standard. For calculations of fold-change between the groups of proteins, total protein abundance values were added together, and the ratios of these sums were used to compare proteins within different samples.

4.8 | Luciferase activity assays

For measuring ER stress, a lentiviral luciferase-reporter vector for CBF/NF-Y/YY1 promoters (ER stress response elements) was purchased (Qiagen, # CLS-9032L) and HPDE-H6c7 or hTERT-HPNE cells were infected according to manufacturer's protocol. Cells were grown for 3 weeks under selection of puromycin until a stable cell line was generated. CBF/NF-Y/YY1 activity was confirmed using tunicamycin treatment as a positive control. To determine our EV preparations were biologically active, a cancer associated fibroblast (CAF) cell line (pCAF2) expressing TGF-β responsive SMAD2/3/4 RE-Luciferase (Qiagen, #CLS-017L) was created. pCAF2 was derived from a patient-derived xenograft (PDX) mouse model of PDAC. Informed consent was obtained from all patients preoperatively under the institutional review board approved protocol IRB201600873 at the University of Florida. Following surgical resection of the patient tumour, a 2×2mm piece of tumour tissue was isolated from the specimen. This was then implanted directly into an 8-week-old female nonobese diabetic severe combined immunodeficient mouse (Jackson Laboratory, Bar Harbor, ME) (Delitto et al., 2015). Cancer associated fibroblasts (CAFs) were isolated as previously described (Han et al., 2015) from xenografts. Tumour tissue was fragmented into 1mm (Siegel et al., 2020) segments. Segments were placed into a 10mM CaCl2/FBS coated six-well plate. CAFs were maintained in culture comprised of Dulbecco's Modified Eagle's Medium-F12 (DMEM-F12), antibiotic antimycotic solution (Fisher Scientific, Waltham, MA), 10% fetal bovine serum (FBS) (Atlanta Biologicals, Atlanta, GA), and 5% CO2 at 37 °C. CAFs were passaged after they had grown to 80% confluence at 2.5×10 (Renz et al., 2017) per 100mm dish. Screening of many lentiviral luciferase constructs (data not shown) for downstream activated targets of cEVs revealed that SMAD2/3/4 genes were consistently significantly upregulated post cEV treatment (Figure S7). Luciferase activity was confirmed using recombinant human TGFβ (R&D Systems, #240-B-010) treatment.

4.9 | Immunoblot for proteomics and UPR validation

For proteomics validations, independent EV isolations were performed from PANC-1, PPCL-68 and HPDE-H6c7 cell lines using ultracentrifugation with filtration as described above. For UPR validation, cells were grown as described above and proteins were collected by lysing cells with M-PER Mammalian Protein Extraction Reagent (ThermoFisher, #7850). Protein concentrations were determined using BCA and, 15–20 μg of protein per sample was resuspended in sample buffer (2x LDS and distilled H2O) + 200 mM DTT (final concentration). EV samples were lyophilized prior to resuspension in sample buffer. Samples were heated at 95°C for 5 min and run on a 4–12% Bis-Tris NuPage gel (Thermo Fisher, #NP0321). Samples were then transferred to PVDF membranes, blocked with 1–3% bovine serum albumin (BSA) in tris buffer saline + 0.01% tween-20 (TBST) for 1 h. Primary antibodies were added, and membranes were incubated according to manufacturer's protocol. Membranes were subsequently washed 3x with TBST, incubated with secondary antibodies for 1 h at room temperature, visualized and representative images were taken. The following antibodies were used from ProteinTech: Anti-TMEM-59 (#24134-1-AP). Anti-TSG101 (#28283-1-AP), Anti-RALA (#13629-1-AP), Anti-UBAC2 (#25122-1-AP), Anti-XBP1u (#25997-1-AP). The following antibodies were used from Cell Signalling Technology: Anti-PERK (#5683), Anti-Phospho-PERK (T980, #3179), Anti-ERN1 (#3294), Anti-DDIT3 (#2895), Anti-ATF6 (#65880), Anti-XBP1s (#40435). Anti-phospho-ERN1 was purchased from Abcam (# ab48187). Anti-phospho-eIF2α (#44-728G) and Anti-GAPDH (#MA5-15738) were purchased from Invitrogen. Anti-RAB40C was purchased from Millipore Sigma (#07-1392).

4.10 | Palmitic acid treatment

Palmitic acid (Sigma, #P0500) was first conjugated to bovine serum albumin (BSA) for intracellular delivery. 0.1282 grams of palmitic acid was dissolved in 100% ethanol (final concentration of 500 mM) and heated at 70°C until dissolved. 10 μL of the 500 mM palmitic acid solution was added to 990 μL of 10% BSA containing KSFM (final concentration of 5 mM). Samples were vortexed and incubated at 55°C for 15 min. Vortexing and heating was repeated once more. Serial dilutions were made in 10% BSA-containing KSFM and warmed to 37°C prior to cell treatment. 5000 HPDE-H6c7-ERSE luciferase cells were seeded in a 24-well plate and grown for 24 h. Cells were then treated with various concentrations of PA-BSA for an additional 24 h before luciferase activity was analysed.

4.11 | Caspase 3/7 activity assay

Two thousand five hundred cells were seeded in a 96-well plate. After 24 h, cells were treated with 1.00×10^9 cEVs and incubated for 48 h. Caspase 3/7 activity was measured using the Caspase-Glo® 3/7 Assay (Promega, # G8090) according to manufacturer's protocol.

4.12 | Live/dead cell fluorescent microscopy

Five thousand cells (hTERT-HPNE or HPDE-H6c7) were seeded in a 96-well plate. After 24 h, cells were treated with 1.00×10^9 cEVs and incubated for an additional 24 h. Cells were then stained with live/dead reagents (Invitrogen, #L3224) according to manufacturer's protocol and the number of dead cells was counted ($n = 3$ wells per condition) and quantified.

4.13 | Quantification of cell number by DAPI staining

Two thousand five hundred cells were seeded in 96-well plates and allow to grow for 24 h. Cells were then treated with 5.00×10^8 cEVs and grown an additional 24 h. To determine total cell number, cells were fixed with methanol, stained with 0.1% DAPI, images were captured under a microscope and cells per treatment were calculated in ImageJ ($n = 3$ wells per condition).

4.14 | Crystal violet staining

Two thousand five hundred cells were seeded in 96-well plates and allow to grow for 24 h. Cells were treated with 5.00×10^8 cEVs and grown an additional 48 h. Cells were stained with Crystal Violet (Sigma, #3886) (0.5%) and counted in ImageJ ($n = 3$ wells per condition).

4.15 | EV internalization

EVs were stained with PKH67 (Sigma, #PKH67-GL-1KT) and unbound dye was removed using 3 kDa MWCO centrifugal filters (Invitrogen, #448449), according to manufacturer's protocol. Dummy samples wherein PKH67 was added to 1 x DPBS without EVs and processed the same as EV samples above were used as a negative control, to account for the formation of dye aggregates. 10,000 hTERT-HPNE or HPDE-H6c7 cells were seeded into a glass bottom 96-well plate. The next day, media was changed and 5 μg (as determined by BCA) of labelled EVs were added to each well. After 24 h, nuclei were stained using Hoechst 33342 dye (Invitrogen, #R37605) according to manufacturer's protocol and representative fluorescent microscopy images were captured using a BZ-X710 (Keyence) fluorescent microscope.

4.15.1 | Confocal microscopy and 3D rendering analysis

hTERT-HPNE or HPDE-H6c7 cells were seeded on glass bottom 35mm dishes and treated as above. Immediately prior to imaging, cell membranes were stained using CellMask Deep Red (ThermoFisher, # C10046) according to manufacturer's protocol, followed by nuclei staining with Hoechst 33342 dye as above. Confocal images were captured (Zeiss Axio Observer 7, LCM700) using the following wavelengths: 650 nm excitation and 673 nm emission for CellMask Deep Red, 493 nm excitation and 517 nm emission for PKH67 and 353 nm excitation and 465 nm emission for Hoechst 33342. A Zeiss Plan-Apochromat 63x/1.40 Oil DIC M27 objective was used for all image acquisition. Z-stack images were acquired in 10 slices (12.96 μm). 3D renders of the acquired Z-stack images were generated using IMARIS (Oxford Instruments).

4.16 | Luminex cytokine assay

HPDE-H6c7 cells were seeded in a 24-well plate with 50,000 cells per well ($n = 4$ per condition). After 24 h, media was changed, and cells were treated with 1×10^{10} cEVs or nEVs. At either 2- or 4-days post initial treatment, media was collected for cytokine analysis. Media was changed every 2 days and cells were re-treated with another dose of either cEVs or nEVs. For collection, media was immediately aspirated from wells and placed into 2 ml centrifuge tubes. Media was cleared by centrifugation for 15 min at 1500 x g. Supernatant was then placed into new tubes and samples were stored at −80°C until Luminex analysis. Luminex 200 (Luminex Corp.) was used to analyse cytokines by multiplex analysis. 48 cytokines were quantified in the cell supernatant using a Bio-Plex Pro Human Cytokine Screening Panel (Bio-Rad, #12007283) according to manufacturer's protocol. Cytokine concentrations (pg/ml) were determined by fluorescence intensity and quantification was obtained using Bio-Plex Manager software, version 6.1 (Bio-Rad).

4.17 | Wound healing scratch assay

70,000 – 100,000 of hTERT-HPNE or HPDE-H6c7 cells were seeded in a 24-well plate and allowed to reach 90–100% confluence. At confluence, a scratch was made in each well using a standard 200 μl pipette tip. Cell culture media was changed, cells were treated as indicated in the figures and images were captured at 0h, 24h and 48h post-treatment. The wound area and wound closure percentage was calculated in ImageJ as described by Suarez-Arnedo and colleagues (Suarez-Arnedo et al., 2020). Time lapse live cell imaging was captured up to 48h at an interval of 15 min per image on a EVOS M5000 Imaging System (ThermoFisher).

4.18 | Violet cell tracing proliferation assay

Cells were stained using the CellTrace Violet Cell Proliferation Kit (Invitrogen, # C34557) according to manufacturers protocol. 30,000 cells were then seeded in 24-well plates and treated as described in each figure. After the treatment period, cells were detached using trypsin and collected by spinning at 1800 x rpm for 5 min. Cells were washed in 1 x PBS and transferred to flow cytometry tubes. Cells were then stained with Helix NP NIR (BioLegend) for live/dead cell sorting, according to manufacturer's protocol. Flow cytometry data was acquired on a BD LSRFortessa by the Flow Cytometry core at Georgetown University Medical Center. Results were analysed using FlowJo (BD Biosciences).

4.19 | Annexin V apoptosis assay

100,000 hTERT-HPNE or HPDE-H6c7 cells were seeded in a 6-well plate and allowed to attach overnight. The next day, media was changed, and treatments were given as indicated in the figures. Cells were allowed to grow for 24h or 48h post-treatment.

At collection, media was collected to conserve dead cells. Adherent cells were detached with trypsin and added to collected media. Cells were spun at 1800 x rpm and the remaining cell pellet was washed with 1 x PBS. Cells were transferred to flow cytometry tubes and dyed with Annexin V-FITC (BD Biosciences, #556547) according to manufacturer's recommendations. Flow cytometry data was acquired on a BD LSRFortessa by the Flow Cytometry core at Georgetown University Medical Center. Results were analysed using FCS Express 7 (De Novo Software).

4.20 | EdU incorporation assay

10,000 hTERT-HPNE or HPDE-H6c7 cells were seeded in 96-well plates and allowed to attach overnight. The next day, cells were treated as indicated in the figures. Proliferation was measured using the Click-iT EdU Proliferation Assay for Microplates (ThermoFisher, #C10499). At the end of the treatment time point, EdU at a final concentration of 10 μM per well was added to the cells. After an additional 18h of incubation, cells were fixed and analysed per manufacturers protocol.

4.21 | Invasion assay

hTERT-HPNE ($N = 5000$) or HPDE-H6c7 ($N = 20{,}000$) cells were seeded in a 24-well Matrigel invasion chamber (Corning, #354480) along with treatments as indicated in the figures. Cells were allowed to invade for 48h, after which they were fixed and stained with crystal violet. Representative images from three fields of view per well were captured (Zeiss AxioPlan 2 Imaging System) and cell invasion was quantified using ImageJ.

4.22 | Data analysis and statistics

Proteomics, metabolomics, lipidomics and RNA-Seq data were pre-processed as described above. All statistical analyses were performed using custom R scripts with log transformation. Significant features were determined using FDR-adjusted ($p < 0.05$) cut-off value. Metabolomics and lipidomics data matrices were normalized using the probabilistic quotient normalization (PQN) method (Dieterle et al., 2006; Li et al., 2016). Features with quality control (QC) sample relative standard deviations (RSD) > 20% were excluded from analysis. Proteomics data was normalized to total intensity. For RNA-Seq, differential expression analysis was performed using the DESeq2 R package (1.14.1). All other reported statistical analyses were binary comparisons using Student's two-tailed *t*-tests with homogenous variance.

ACKNOWLEDGEMENTS

Our immense thanks to Drs. Maryna Baydyuk, Mi-Hye Lee and Jeff Huang for providing access to and assistance with the confocal microscopy image acquisition. Many thanks to Mr. Phil Gross for assisting us with IMARIS 3D rendering of said confocal microscopy images. We also thank Dr. Pankaj Gaur for assisting us with analysis of our flow cytometry data. Sincerest thanks to Dr. Dean Rosenthal, Dr. Cynthia-Simbulan Rosenthal, Ms. Yoga Haribabu and Ms. Nusrat Islam for access to and assistance with live cell time lapse microscopy. We would additionally thank the Metabolomics Shared Resource, Flow Cytometry & Cell Sorting Shared Resource and Genomics & Epigenomics Shared Resource at Georgetown University, all partially supported by NIH/NCI grant P30-CA051008. We would also like to thank Dr. Kelly Dryden from the University of Virginia. Transmission electron micrographs were recorded at the University of Virginia Molecular Electron Microscopy Core facility (RRID:SCR_019031), which is supported in part by the School of Medicine and built with NIH grant G20-RR31199. Experimental schematics were created with BioRender.com. Finally, we would express deep gratitude to the anonymous reviewers of our manuscript, for their input that helped improve the quality and impact of this study significantly. This study was supported by the American Cancer Society (IRG-92-152-17 award number AWD4470404), Georgetown Lombardi Comprehensive Cancer Center Support Grant Developmental Funds and the Ruesch Foundation to A.K.C and by the National Center for Advancing Translational Sciences of the National Institutes of Health under Award Number TL1TR001431, and a Cosmos Scholars Grant from the Cosmos Club Foundation to Charles P. Hinzman. The content is solely the responsibility of the authors and does not necessarily represent the official views of the National Institutes of Health. The opinions or assertions contained herein are the private views of the authors and are not necessarily those of the Uniformed Services University of the Health Sciences, or the Department of Defense, USA.

CONFLICT OF INTERESTS

The authors declare no competing interests. The authors alone are responsible for the content and writing of this paper.

AUTHOR CONTRIBUTIONS

Charles P. Hinzman, Shivani Bansal, Anton Iliuk, Baldev Singh, Kelly M. Herremans, Jose G. Trevino, Vijay K. Singh and Partha P. Banerjee were responsible for data collection. Charles P. Hinzman, Baldev Singh, Yaoxiang Li, and Michael Girgis were

responsible for data analysis and interpretation. Charles P. Hinzman, Partha P. Banerjee, and Amrita K. Cheema were responsible for drafting and editing of the manuscript as well as for the conception and design of the work.

MATERIALS AND CORRESPONDENCE

Raw proteomics data has been deposited to the Proteomics Identifications Database (PRIDE) under accession number PXD028597. Raw RNA-Seq data has been deposited to the Gene Expression Omnibus (GEO) database under accession number GSE181625. All other requests for materials, data and reagents used in this study will be fulfilled by the corresponding author.

ORCID

Charles P. Hinzman https://orcid.org/0000-0002-4669-4357
Yaoxiang Li https://orcid.org/0000-0001-9200-1016
Amrita K. Cheema https://orcid.org/0000-0003-4877-7583

REFERENCES

Allenson, K., Castillo, J., San Lucas, F. A., Scelo, G., Kim, D. U., Bernard, V., Davis, G., Kumar, T., Katz, M., Overman, M. J., Foretova, L., Fabianova, E., Holcatova, I., Janout, V., Meric-Bernstam, F., Gascoyne, P., Wistuba, I., Varadhachary, G., Brennan, P., … Alvarez, H. (2017). High prevalence of mutant KRAS in circulating exosome-derived DNA from early-stage pancreatic cancer patients. *Annals of Oncology*, *28*, 741–747. https://doi.org/10.1093/annonc/mdx004

Babst, M., Odorizzi, G., Estepa, E. J., & Emr, S. D. (2000). Mammalian tumor susceptibility gene 101 (TSG101) and the yeast homologue, Vps23p, both function in late endosomal trafficking. *Traffic (Copenhagen, Denmark)*, *1*, 248–258. https://doi.org/10.1034/j.1600-0854.2000.010307.x

Balachandran, V. P., Beatty, G. L., & Dougan, S. K. (2019). Broadening the impact of immunotherapy to pancreatic cancer: Challenges and opportunities. *Gastroenterology*, *156*, 2056–2072. https://doi.org/10.1053/j.gastro.2018.12.038

Basseri, S., & Austin, R. C. (2012). Endoplasmic reticulum stress and lipid metabolism: mechanisms and therapeutic potential. *Biochemistry Research International*, *1-13*, 841362. https://doi.org/10.1155/2012/841362

Ben-Dror, K., & Birk, R. (2019). Oleic acid ameliorates palmitic acid-induced ER stress and inflammation markers in naive and cerulein-treated exocrine pancreas cells. *Bioscience Reports*, *39*, BSR20190054. https://doi.org/10.1042/BSR20190054

Blando, J., Sharma, A., Higa, M. G., Zhao, H., Vence, L., Yadav, S. S., Kim, J., Sepulveda, A. M., Sharp, M., Maitra, A., Wargo, J., Tetzlaff, M., Broaddus, R., Katz, M. H. G., Varadhachary, G. R., Overman, M., Wang, H., Yee, C., Bernatchez, C., … Sharma, P. (2019). Comparison of immune infiltrates in melanoma and pancreatic cancer highlights VISTA as a potential target in pancreatic cancer. *PNAS*, *116*, 1692–1697. https://doi.org/10.1073/pnas.1811067116

Bouvy, C., Gheldof, D., Chatelain, C., Mullier, F., & Dogné, J.-M. (2014). Contributing role of extracellular vesicles on vascular endothelium haemostatic balance in cancer. *Journal of Extracellular Vesicles*, *3*, 24400. https://doi.org/10.3402/jev.v3.24400

Cao, Y., Trillo-Tinoco, J., Sierra, R. A., Anadon, C., Dai, W., Mohamed, E., Cen, L., Costich, T. L., Magliocco, A., Marchion, D., Klar, R., Michel, S., Jaschinski, F., Reich, R. R., Mehrotra, S., Cubillos-Ruiz, J. R., Munn, D. H., Conejo-Garcia, J. R., & Rodriguez, P. C. (2019). ER stress-induced mediator C/EBP homologous protein thwarts effector T cell activity in tumors through T-bet repression. *Nature Communication*, *10*, 1280. https://doi.org/10.1038/s41467-019-09263-1

Castranova, D., Davis, A. E., Lo, B. D., Miller, M. F., Paukstelis, P. J., Swift, M. R., Pham, V. N., Torres-Vázquez, J., Bell, K., Shaw, K. M., Kamei, M., & Weinstein, B. M. (2016). Aminoacyl-transfer RNA Synthetase deficiency promotes angiogenesis via the unfolded protein response pathway. *Arteriosclerosis, Thrombosis, and Vascular Biology*, *36*, 655–662. https://doi.org/10.1161/ATVBAHA.115.307087

Chang, Y. T., Peng, H.-Y., Hu, C.-M., Huang, S.-C., Tien, S.-C., & Jeng, Y.-M. (2020). Pancreatic cancer-derived small extracellular vesical Ezrin regulates macrophage polarization and promotes metastasis. *American Journal of Cancer Research*, *10*, 12–37.

Chen, E. Y., Tan, C. M., Kou, Y., Duan, Q., Wang, Z., Meirelles, G. V., Clark, N. R., & Ma'ayan, A. (2013). Enrichr: interactive and collaborative HTML5 gene list enrichment analysis tool. *Bmc Bioinformatics [Electronic Resource]*, *14*, 128. https://doi.org/10.1186/1471-2105-14-128

Cicenas, J., Kvederaviciute, K., Meskinyte, I., Meskinyte-Kausiliene, E., Skeberdyte, A., & Cicenas, J. (2017). KRAS, TP53, CDKN2A, SMAD4, BRCA1, and BRCA2 Mutations in Pancreatic Cancer. *Cancers (Basel)*, *9*, 42. https://doi.org/10.3390/cancers9050042

Clarke, R., Cook, K. L., Hu, R., Facey, C. O. B., Tavassoly, I., Schwartz, J. L., Baumann, W. T., Tyson, J. J., Xuan, J., Wang, Y., Wärri, A., & Shajahan, A. N. (2012). Endoplasmic reticulum stress, the unfolded protein response, autophagy, and the integrated regulation of breast cancer cell fate. *Cancer Research*, *72*, 1321–1331. https://doi.org/10.1158/0008-5472.CAN-11-3213

Clos-Garcia, M., Loizaga-Iriarte, A., Zuñiga-Garcia, P., Sánchez-Mosquera, P., Rosa Cortazar, A., González, E., Torrano, V., Alonso, C., Pérez-Cormenzana, M., Ugalde-Olano, A., Lacasa-Viscasillas, I., Castro, A., Royo, F., Unda, M., Carracedo, A., & Falcón-Pérez, J. M. (2018). Metabolic alterations in urine extracellular vesicles are associated to prostate cancer pathogenesis and progression. *Journal of Extracellular Vesicles*, *7*, 1470442. https://doi.org/10.1080/20013078.2018.1470442

Costa-Silva, B., Aiello, N. M., Ocean, A. J., Singh, S., Zhang, H., Thakur, B. K., Becker, A., Hoshino, A., Mark, M. T., Molina, H., Xiang, J., Zhang, T., Theilen, T.-M., García-Santos, G., Williams, C., Ararso, Y., Huang, Y., Rodrigues, G., Shen, T.-L., … Lyden, D. (2015). Pancreatic cancer exosomes initiate pre-metastatic niche formation in the liver. *Nature Cell Biology*, *17*, 816–826. https://doi.org/10.1038/ncb3169

Cubillos-Ruiz, J. R., Bettigole, S. E., & Glimcher, L. H. (2017). Tumorigenic and Immunosuppressive Effects of Endoplasmic Reticulum Stress in Cancer. *Cell*, *168*, 692–706. https://doi.org/10.1016/j.cell.2016.12.004

Danino, H., Ben-Dror, K., & Birk, R. (2015). Exocrine pancreas ER stress is differentially induced by different fatty acids. *Experimental Cell Research*, *339*, 397–406. https://doi.org/10.1016/j.yexcr.2015.09.022

Delitto, D., Pham, K., Vlada, A. C., Sarosi, G. A., Thomas, R. M., Behrns, K. E., Liu, C., Hughes, S. J., Wallet, S. M., & Trevino, J. G. (2015). Patient-derived xenograft models for pancreatic adenocarcinoma demonstrate retention of tumor morphology through incorporation of murine stromal elements. *American Journal of Pathology*, *185*, 1297–1303. https://doi.org/10.1016/j.ajpath.2015.01.016

Dieterle, F., Ross, A., Schlotterbeck, G., & Senn, H. (2006). Probabilistic quotient normalization as robust method to account for dilution of complex biological mixtures. Application in 1H NMR metabonomics. *Analytical Chemistry*, *78*, 4281–4290. https://doi.org/10.1021/ac051632c

Dumartin, L., Alrawashdeh, W., Trabulo, S. M., Radon, T. P., Steiger, K., Feakins, R. M., Di Magliano, M. P., Heeschen, C., Esposito, I., Lemoine, N. R., & Crnogorac-Jurcevic, T. (2017). ER stress protein AGR2 precedes and is involved in the regulation of pancreatic cancer initiation. *Oncogene*, *36*, 3094–3103. https://doi.org/10.1038/onc.2016.459

El Andaloussi, S., Mäger, I., Breakefield, X. O., & Wood, M. J. A. (2013). Extracellular vesicles: biology and emerging therapeutic opportunities. *Nature Reviews Drug Discovery*, *12*, 347–357. https://doi.org/10.1038/nrd3978

Elyada, E., Bolisetty, M., Laise, P., Flynn, W. F., Courtois, E. T., Burkhart, R. A., Teinor, J. A., Belleau, P., Biffi, G., Lucito, M. S., Sivajothi, S., Armstrong, T. D., Engle, D. D., Yu, K. H., Hao, Y., Wolfgang, C. L., Park, Y., Preall, J., Jaffee, E. M., … Tuveson, D. A. (2019). Cross-species single-cell analysis of pancreatic ductal adenocarcinoma reveals antigen-presenting cancer-associated fibroblasts. *Cancer Discovery*, *9*, 1102–1123. https://doi.org/10.1158/2159-8290.CD-19-0094

Gow, A., & Wrabetz, L. (2009). CHOP and the endoplasmic reticulum stress response in myelinating glia. *Current Opinion in Neurobiology*, *19*, 505–510. https://doi.org/10.1016/j.conb.2009.08.007

Guan, X., Deng, H., Choi, U. L., Li, Z., Yang, Y., Zeng, J., Liu, Y., Zhang, X., & Li, G. (2020). EZH2 overexpression dampens tumor-suppressive signals via an EGR1 silencer to drive breast tumorigenesis. *Oncogene*, *39*, 7127–7141. https://doi.org/10.1038/s41388-020-01484-9

Halterman, M. W., Gill, M., Dejesus, C., Ogihara, M., Schor, N. F., & Federoff, H. J. (2010). The endoplasmic reticulum stress response factor CHOP-10 protects against hypoxia-induced neuronal death. *Journal of Biological Chemistry*, *285*, 21329–21340. https://doi.org/10.1074/jbc.M109.095299

Han, S., Delitto, D., Zhang, D., Sorenson, H. L., Sarosi, G. A., Thomas, R. M., Behrns, K. E., Wallet, S. M., Trevino, J. G., & Hughes, S. J. (2015). Primary outgrowth cultures are a reliable source of human pancreatic stellate cells. *Laboratory Investigation*, *95*, 1331–1340. https://doi.org/10.1038/labinvest.2015.117

Hartwig, W., Werner, J., Jäger, D., Debus, J., & Büchler, M. W. (2013). Improvement of surgical results for pancreatic cancer. *The Lancet Oncology*, *14*, e476–e485. https://doi.org/10.1016/S1470-2045(13)70172-4

Hatanaka, M., Maier, B., Sims, E. K., Templin, A. T., Kulkarni, R. N., Evans-Molina, C., & Mirmira, R. G. (2014). Palmitate induces mRNA translation and increases ER protein load in islet beta-cells via activation of the mammalian target of rapamycin pathway. *Diabetes*, *63*, 3404–3415. https://doi.org/10.2337/db14-0105

Heinz, S., Benner, C., Spann, N., Bertolino, E., Lin, Y. C., Laslo, P., Cheng, J. X., Murre, C., Singh, H., & Glass, C. K. (2010). Simple combinations of lineage-determining transcription factors prime cis-regulatory elements required for macrophage and B cell identities. *Molecular Cell*, *38*, 576–589. https://doi.org/10.1016/j.molcel.2010.05.004

Hess, D. A., Humphrey, S. E., Ishibashi, J., Damsz, B., Lee, A.-H., Glimcher, L. H., & Konieczny, S. F. (2011). Extensive pancreas regeneration following acinar-specific disruption of Xbp1 in mice. *Gastroenterology*, *141*, 1463–1472. https://doi.org/10.1053/j.gastro.2011.06.045

Hetz, C. (2012). The unfolded protein response: controlling cell fate decisions under ER stress and beyond. *Nature Reviews Molecular Cell Biology*, *13*, 89–102. https://doi.org/10.1038/nrm3270

Hetz, C., & Papa, F. R. (2018). The unfolded protein response and cell fate control. *Molecular Cell*, *69*, 169–181. https://doi.org/10.1016/j.molcel.2017.06.017

Hu, H., Tian, M., Ding, C., & Yu, S. (2018). The C/EBP Homologous Protein (CHOP) transcription factor functions in endoplasmic reticulum stress-induced apoptosis and microbial infection. *Frontiers in Immunology*, *9*, 3083. https://doi.org/10.3389/fimmu.2018.03083

Kajiwara, K., Muneoka, T., Watanabe, Y., Karashima, T., Kitagaki, H., & Funato, K. (2012). Perturbation of sphingolipid metabolism induces endoplasmic reticulum stress-mediated mitochondrial apoptosis in budding yeast. *Molecular Microbiology*, *86*, 1246–1261. https://doi.org/10.1111/mmi.12056

Karaskov, E., Scott, C., Zhang, L., Teodoro, T., Ravazzola, M., & Volchuk, A. (2006). Chronic palmitate but not oleate exposure induces endoplasmic reticulum stress, which may contribute to INS-1 pancreatic beta-cell apoptosis. *Endocrinology*, *147*, 3398–3407. https://doi.org/10.1210/en.2005-1494

Katzmann, D. J., Odorizzi, G., & Emr, S. D. (2002). Receptor downregulation and multivesicular-body sorting. *Nature Reviews Molecular Cell Biology*, *3*, 893–905. https://doi.org/10.1038/nrm973

Kong, Y., Zhao, X., Qiu, M., Lin, Y., Feng, P., Li, S., Liang, B., Zhu, Q., Huang, H., Li, C., & Wang, W. (2021). Tubular Mas receptor mediates lipid-induced kidney injury. *Cell Death & Disease*, *12*, 110. https://doi.org/10.1038/s41419-020-03375-z

Kuleshov, M. V., Jones, M. R., Rouillard, A. D., Fernandez, N. F., Duan, Q., Wang, Z., Koplev, S., Jenkins, S. L., Jagodnik, K. M., Lachmann, A., Mcdermott, M. G., Monteiro, C. D., Gundersen, G. W., & Ma'ayan, A. (2016). Enrichr: A comprehensive gene set enrichment analysis web server 2016 update. *Nucleic Acids Research*, *44*, W90–W97. https://doi.org/10.1093/nar/gkw377

Lennon, K. M., Wakefield, D. L., Maddox, A. L., Brehove, M. S., Willner, A. N., Garcia-Mansfield, K., Meechoovet, B., Reiman, R., Hutchins, E., Miller, M. M., Goel, A., Pirrotte, P., Van Keuren-Jensen, K., & Jovanovic-Talisman, T. (2019). Single molecule characterization of individual extracellular vesicles from pancreatic cancer. *Journal of Extracellular Vesicles*, *8*, 1685634. https://doi.org/10.1080/20013078.2019.1685634

Li, B., Tang, J., Yang, Q., Cui, X., Li, S., Chen, S., Cao, Q., Xue, W., Chen, N., & Zhu, F. (2016). Performance evaluation and online realization of data-driven normalization methods used in LC/MS based untargeted metabolomics analysis. *Science Reports*, *6*, 38881. https://doi.org/10.1038/srep38881

Lu, M., Lawrence, D. A., Marsters, S., Acosta-Alvear, D., Kimmig, P., Mendez, A. S., Paton, A. W., Paton, J. C., Walter, P., & Ashkenazi, A. (2014). Opposing unfolded-protein-response signals converge on death receptor 5 to control apoptosis. *Science*, *345*, 98–101. https://doi.org/10.1126/science.1254312

Maacha, S., Bhat, A. A., Jimenez, L., Raza, A., Haris, M., Uddin, S., & Grivel, J.-C. (2019). Extracellular vesicles-mediated intercellular communication: roles in the tumor microenvironment and anti-cancer drug resistance. *Molecular Cancer*, *18*, 55. https://doi.org/10.1186/s12943-019-0965-7

Madden, E., Logue, S. E., Healy, S. J., Manie, S., & Samali, A. (2019). The role of the unfolded protein response in cancer progression: From oncogenesis to chemoresistance. *Biologie Cellulaire*, *111*, 1–17. https://doi.org/10.1111/boc.201800050

Masamune, A., Kikuta, K., Watanabe, T., Satoh, K., Hirota, M., & Shimosegawa, T. (2008). Hypoxia stimulates pancreatic stellate cells to induce fibrosis and angiogenesis in pancreatic cancer. *American Journal of Physiology Gastrointestinal and Liver Physiology*, *295*, G709–G717. https://doi.org/10.1152/ajpgi.90356.2008

Moncan, M., Mnich, K., Blomme, A., Almanza, A., Samali, A., & Gorman, A. M. (2021). Regulation of lipid metabolism by the unfolded protein response. *Journal of Cellular and Molecular Medicine*, *25*, 1359–1370. https://doi.org/10.1111/jcmm.16255

Morin, E., Sjöberg, E., Tjomsland, V., Testini, C., Lindskog, C., Franklin, O., Sund, M., Öhlund, D., Kiflemariam, S., Sjöblom, T., & Claesson-Welsh, L. (2018). VEGF receptor-2/neuropilin 1 trans-complex formation between endothelial and tumor cells is an independent predictor of pancreatic cancer survival. *Journal of Pathology*, *246*, 311–322. https://doi.org/10.1002/path.5141

Neesse, A., Michl, P., Frese, K. K., Feig, C., Cook, N., Jacobetz, M. A., Lolkema, M. P., Buchholz, M., Olive, K. P., Gress, T. M., & Tuveson, D. A. (2011). Stromal biology and therapy in pancreatic cancer. *Gut*, *60*, 861–868. https://doi.org/10.1136/gut.2010.226092

Öhlund, D., Handly-Santana, A., Biffi, G., Elyada, E., Almeida, A. S., Ponz-Sarvise, M., Corbo, V., Oni, T. E., Hearn, S. A., Lee, E. J., Chio, I. I. C., Hwang, C.-I. l., Tiriac, H., Baker, L. A., Engle, D. D., Feig, C., Kultti, A., Egeblad, M., Fearon, D. T., … Tuveson, D. A. (2017). Distinct populations of inflammatory fibroblasts and myofibroblasts in pancreatic cancer. *Journal of Experimental Medicine*, *214*, 579–596. https://doi.org/10.1084/jem.20162024

Padoan, A., Plebani, M., & Basso, D. (2019). Inflammation and pancreatic cancer: Focus on metabolism, cytokines, and immunity. *International Journal of Molecular Sciences*, *20*, 676 https://doi.org/10.3390/ijms20030676

Pham, K., Delitto, D., Knowlton, A. E., Hartlage, E. R., Madhavan, R., Gonzalo, D. H., Thomas, R. M., Behrns, K. E., George, T. J., Hughes, S. J., Wallet, S. M., Liu, C., & Trevino, J. G. (2016). Isolation of pancreatic cancer cells from a patient-derived xenograft model allows for practical expansion and preserved heterogeneity in culture. *American Journal of Pathology*, *186*, 1537–1546. https://doi.org/10.1016/j.ajpath.2016.02.009

Pužar Dominkuš, P., Stenovec, M., Sitar, S., Lasič, E., Zorec, R., Plemenitaš, A., Žagar, E., Kreft, M., & Lenassi, M. (2018). PKH26 labeling of extracellular vesicles: Characterization and cellular internalization of contaminating PKH26 nanoparticles. *Biochim Biophys Acta Biomembr*, *1860*, 1350–1361. https://doi.org/10.1016/j.bbamem.2018.03.013

Quante, A. S., Ming, C., Rottmann, M., Engel, J., Boeck, S., Heinemann, V., Westphalen, C. B., & Strauch, K. (2016). Projections of cancer incidence and cancer-related deaths in Germany by 2020 and 2030. *Cancer Medicine*, *5*, 2649–2656. https://doi.org/10.1002/cam4.767

Rahib, L., Smith, B. D., Aizenberg, R., Rosenzweig, A. B., Fleshman, J. M., & Matrisian, L. M. (2014). Projecting cancer incidence and deaths to 2030: the unexpected burden of thyroid, liver, and pancreas cancers in the United States. *Cancer Research*, *74*, 2913–2921. https://doi.org/10.1158/0008-5472.CAN-14-0155

Record, M., Silvente-Poirot, S., Poirot, M., & Wakelam, M. O. (2018). Extracellular vesicles: lipids as key components of their biogenesis and functions. *Journal of Lipid Research*, *59*, 1316–1324. https://doi.org/10.1194/jlr.E086173

Renz, B. W., Boeck, S., Roeder, F., Trumm, C., Heinemann, V., & Werner, J. (2017). Oligometastatic disease in pancreatic cancer - How to proceed? *Visceral Medicine*, *33*, 36–41. https://doi.org/10.1159/000455027

Riahi, Y., Israeli, T., Cerasi, E., & Leibowitz, G. (2018). Effects of proinsulin misfolding on beta-cell dynamics, differentiation and function in diabetes. *Diabetes, Obesity & Metabolism*, *20*, 95–103. https://doi.org/10.1111/dom.13379

Richards, K. E., Zeleniak, A. E., Fishel, M. L., Wu, J., Littlepage, L. E., & Hill, R. (2017). Cancer-associated fibroblast exosomes regulate survival and proliferation of pancreatic cancer cells. *Oncogene*, *36*, 1770–1778. https://doi.org/10.1038/onc.2016.353

Sah, R. P., Garg, S. K., Dixit, A. K., Dudeja, V., Dawra, R. K., & Saluja, A. K. (2014). Endoplasmic reticulum stress is chronically activated in chronic pancreatitis. *Journal of Biological Chemistry*, *289*, 27551–27561. https://doi.org/10.1074/jbc.M113.528174

Shah, R., Patel, T., & Freedman, J. E. (2018). Circulating extracellular vesicles in human disease. *The New England journal of medicine*, *379*, 958–966. https://doi.org/10.1056/NEJMra1704286

Siegel, R. L., Miller, K. D., & Jemal, A. (2020). Cancer statistics, 2020. *CA: A Cancer Journal for Clinicians*, *70*, 7–30. https://doi.org/10.3322/caac.21590

Simonsen, J. B. (2019). Pitfalls associated with lipophilic fluorophore staining of extracellular vesicles for uptake studies. *Journal of Extracellular Vesicles*, *8*, 1582237. https://doi.org/10.1080/20013078.2019.1582237

Snel, B. (2000). STRING: a web-server to retrieve and display the repeatedly occurring neighbourhood of a gene. *Nucleic Acids Research*, *28*, 3442–3444. https://doi.org/10.1093/nar/28.18.3442

Suarez-Arnedo, A., Torres Figueroa, F., Clavijo, C., Arbeláez, P., Cruz, J. C., & Muñoz-Camargo, C. (2020). An image J plugin for the high throughput image analysis of in vitro scratch wound healing assays. *Plos One*, *15*, e0232565. https://doi.org/10.1371/journal.pone.0232565

Szklarczyk, D., Gable, A. L., Nastou, K. C., Lyon, D., Kirsch, R., Pyysalo, S., Doncheva, N. T., Legeay, M., Fang, T., Bork, P., Jensen, L. J., & Von Mering, C. (2021). The STRING database in 2021: customizable protein-protein networks, and functional characterization of user-uploaded gene/measurement sets. *Nucleic Acids Research*, *49*, D605–D612. https://doi.org/10.1093/nar/gkaa1074

Takov, K., Yellon, D. M., & Davidson, S. M. (2017). Confounding factors in vesicle uptake studies using fluorescent lipophilic membrane dyes. *Journal of Extracellular Vesicles*, *6*, 1388731. https://doi.org/10.1080/20013078.2017.1388731

Tao, L., Zhou, J., Yuan, C., Zhang, L., Li, D., Si, D., Xiu, D., & Zhong, L. (2019). Metabolomics identifies serum and exosomes metabolite markers of pancreatic cancer. *Metabolomics*, *15*, 86. https://doi.org/10.1007/s11306-019-1550-1

Tkach, M., & Théry, C. (2016). Communication by extracellular vesicles: Where we are and where we need to go. *Cell*, *164*, 1226–1232. https://doi.org/10.1016/j.cell.2016.01.043

Urra, H., Dufey, E., Avril, T., Chevet, E., & Hetz, C. (2016). Endoplasmic reticulum stress and the hallmarks of cancer. *Trends in Cancer*, *2*, 252–262. https://doi.org/10.1016/j.trecan.2016.03.007

Van Deun, J., Mestdagh, P., Agostinis, P., Akay, Ö., Anand, S., Anckaert, J., Martinez, Z. A., Baetens, T., Beghein, E., Bertier, L., Berx, G., Boere, J., Boukouris, S., Bremer, M., Buschmann, D., Byrd, J. B., Casert, C., Cheng, L., Cmoch, A., … Vandesompele, J. (2017). An Hendrix EV-TRACK: transparent reporting and centralizing knowledge in extracellular vesicle research. *Nature Methods*, *14*, 228–232. https://doi.org/10.1038/nmeth.4185

Vennin, C., Mélénec, P., Rouet, R., Nobis, M., Cazet, A. S., Murphy, K. J., Herrmann, D., Reed, D. A., Lucas, M. C., Warren, S. C., Elgundi, Z., Pinese, M., Kalna, G., Roden, D., Samuel, M., Zaratzian, A., Grey, S. T., Da Silva, A., Leung, W., … Timpson, P. (2019). CAF hierarchy driven by pancreatic cancer cell p53-status creates a pro-metastatic and chemoresistant environment via perlecan. *Nature Communication*, *10*, 3637. https://doi.org/10.1038/s41467-019-10968-6

Weston-Green, K., Babic, I., De Santis, M., Pan, B., Montgomery, M. K., Mitchell, T., Huang, X.-F., & Nealon, J. (2018). Disrupted sphingolipid metabolism following acute clozapine and olanzapine administration. *Journal of Biomedical Science*, *25*, 40. https://doi.org/10.1186/s12929-018-0437-1

Williams, C., Palviainen, M., Reichardt, N. - C., Siljander, P. R.-M., & Falcón-Pérez, J. M. (2019). Metabolomics applied to the study of extracellular vesicles. *Metabolites*, *9*, 276. https://doi.org/10.3390/metabo9110276

Willms, E., Cabañas, C., Mäger, I., Wood, M. J. A., & Vader, P. (2018). Extracellular vesicle heterogeneity: Subpopulations, isolation techniques, and diverse functions in cancer progression. *Frontiers in Immunology*, *9*, 738. https://doi.org/10.3389/fimmu.2018.00738

Willms, E., Johansson, H. J., Mäger, I., Lee, Y., Blomberg, K. E. M., Sadik, M., Alaarg, A., Smith, C. I. E., Lehtiö, J., El Andaloussi, S., Wood, M. J. A., & Vader, P. (2016). Cells release subpopulations of exosomes with distinct molecular and biological properties. *Science Reports*, *6*, 22519. https://doi.org/10.1038/srep22519

Wu, X., Li, L., Iliuk, A., & Tao, W. A (2018). Highly efficient phosphoproteome capture and analysis from urinary extracellular vesicles. *Journal of Proteome Research*, *17*, 3308–3316. https://doi.org/10.1021/acs.jproteome.8b00459

Xiao, F., Li, H., Feng, Z., Huang, L., Kong, L., Li, M., Wang, D., Liu, F., Zhu, Z., Wei, Y. G., & Zhang, W. (2021). Intermedin facilitates hepatocellular carcinoma cell survival and invasion via ERK1/2-EGR1/DDIT3 signaling cascade. *Science Reports*, *11*, 488. https://doi.org/10.1038/s41598-020-80066-x

Xu, R., Rai, A., Chen, M., Suwakulsiri, W., Greening, D. W., & Simpson, R. J. (2018). Extracellular vesicles in cancer - implications for future improvements in cancer care. *Nature Reviews Clinical Oncology*, *15*, 617–638. https://doi.org/10.1038/s41571-018-0036-9

Yáñez-Mó, M., Siljander, P. R.-M., Andreu, Z., Bedina Zavec, A., Borràs, F. E., Buzas, E. I., Buzas, K., Casal, E., Cappello, F., Carvalho, J., Colás, E., Cordeiro-Da Silva, A., Fais, S., Falcon-Perez, J. M., Ghobrial, I. M., Giebel, B., Gimona, M., Graner, M., Gursel, I., … De Wever, O. (2015). Biological properties of extracellular vesicles and their physiological functions. *Journal of Extracellular Vesicles*, *4*, 27066. https://doi.org/10.3402/jev.v4.27066

Yao, Y., Lu, Q., Hu, Z., Yu, Y., Chen, Q., & Wang, Q. K. (2017). A non-canonical pathway regulates ER stress signaling and blocks ER stress-induced apoptosis and heart failure. *Nature Communication*, *8*, 133. https://doi.org/10.1038/s41467-017-00171-w

Yin, Z., Ma, T., Huang, B., Lin, L., Zhou, Y., Yan, J., Zou, Y., & Chen, S. (2019). Macrophage-derived exosomal microRNA-501-3p promotes progression of pancreatic ductal adenocarcinoma through the TGFBR3-mediated TGF-beta signaling pathway. *Journal of Experimental & Clinical Cancer Research*, *38*, 310. https://doi.org/10.1186/s13046-019-1313-x

Yoshida, H., Matsui, T., Yamamoto, A., Okada, T., & Mori, K. (2001). XBP1 mRNA is induced by ATF6 and spliced by IRE1 in response to ER stress to produce a highly active transcription factor. *Cell*, *107*, 881–891. https://doi.org/10.1016/s0092-8674(01)00611-0

Yu, S., Li, Y., Liao, Z., Wang, Z., Wang, Z., Li, Y., Qian, L., Zhao, J., Zong, H., Kang, B., Zou, W.-B., Chen, K., He, X., Meng, Z., Chen, Z., Huang, S., & Wang, P. (2020). Plasma extracellular vesicle long RNA profiling identifies a diagnostic signature for the detection of pancreatic ductal adenocarcinoma. *Gut*, *69*, 540–550. https://doi.org/10.1136/gutjnl-2019-318860

Zhao, H., Yang, L., Baddour, J., Achreja, A., Bernard, V., Moss, T., Marini, J. C., Tudawe, T., Seviour, E. G., San Lucas, F. A., Alvarez, H., Gupta, S., Maiti, S. N., Cooper, L., Peehl, D., Ram, P. T., Maitra, A., & Nagrath, D. (2016). Tumor microenvironment derived exosomes pleiotropically modulate cancer cell metabolism. *Elife*, *5*, e10250. https://doi.org/10.7554/eLife.10250

Zheng, Z. (2010). Role of unfolded protein response in lipogenesis. *World Journal of Hepatology*, *2*, 203–207. https://doi.org/10.4254/wjh.v2.i6.203

SUPPORTING INFORMATION

Additional supporting information can be found online in the Supporting Information section at the end of this article.

How to cite this article: Hinzman, C. P., Singh, B., Bansal, S., Li, Y., Iliuk, A., Girgis, M., Herremans, K. M., Trevino, J. G., Singh, V. K., Banerjee, P. P., & Cheema, A. K. (2022). A multi-omics approach identifies pancreatic cancer cell extracellular vesicles as mediators of the unfolded protein response in normal pancreatic epithelial cells. *Journal of Extracellular Vesicles*, *11,* e12232. https://doi.org/10.1002/jev2.12232